A CLOSED-LOOP VISUAL STIMULATION FRAMEWORK VIA EEG-BASED CONTROLLABLE GENERATION

Anonymous authors
Paper under double-blind review

ABSTRACT

Recent advancements in artificial neural networks (ANNs) have greatly enhanced the ability to predict neural activity in response to visual stimuli. However, the inverse problem of designing visual stimuli to elicit specific neural responses remains challenging due to high experimental costs, the high dimensionality of stimuli, and incomplete understanding of neural selectivity. To address these limitations, we present a **closed-loop visual stimulation framework via electroencephalography (EEG)-based controllable generation**. It can iteratively generate the optimal visual stimuli to achieve the goal of controlling brain signals. This framework employs an EEG encoder, treated as a non-differentiable black-box model, to predict neural responses evoked by visual stimuli. By utilizing this encoder (or human experiment), we can quantify the similarity between the predicted (or recorded) neural responses and target neural states. Combining EEG feature extraction with a generation/retrieval module, the framework systematically explores large-scale natural image spaces to identify stimuli that optimally align with the desired brain state. Experimental results demonstrate that, irrespective of the precision of ANN-predicted brain activity, our framework efficiently converges to the theoretically optimal stimulus within a fixed number of iterations. Moreover, this framework generalizes effectively across diverse target neural activity patterns, underscoring its robustness and potential for broader applications in brain-inspired stimulus design. Our code is available at `https://anonymous.4open.science/status/closed-loop-F2E9`.

1 INTRODUCTION

The visual system exhibits selectivity, meaning different visual stimuli evoke distinct neural responses (Epstein & Kanwisher, 1998; Qiu et al., 2023). This property suggests that visual stimuli could, in principle, be designed to elicit specific neural responses, offering a novel, non-invasive approach to neuromodulation. Such neuromodulation technique offers several advantages: it is user-friendly, natural, and inherently well-aligned with human sensory processing. However, achieving precise neuromodulation through visual stimuli is highly challenging due to the high dimensionality of visual input space and our incomplete understanding of neuronal selectivity in visual system. Recent advances in controllable image generation techniques have enabled the creation of images with specific semantic attributes, typically conditioned on textual descriptions (Li et al., 2019; Epstein et al., 2023; Wei et al., 2024). While this represents a significant technological breakthrough, current methods lack the ability to conditionally generate stimuli based on neural states. To address this limitation, it is essential to develop frameworks capable of generating visual stimuli specifically optimized to modulate neural activity in a targeted manner, paving the way for more effective and precise neuromodulation through visual stimulation.

Many efforts have focused on precise control of brain activity through visual stimulation. For example, several works (Ponce et al., 2019; Walker et al., 2019; Bashivan et al., 2019) have sought to regulate neural activity at the neuronal level using targeted visual inputs. Notably, (Ponce et al., 2019) introduced a closed-loop experimental framework that integrates a deep generative neural network (GAN) with neurofeedback to iteratively generate images optimized to maximize the responses of specific neurons in the visual system. Despite their success in monkey experiments, these methods often lack generalizability and fail to capture the full diversity of visual features due to the small number of trials and constraints inherent in animal experiments. Moreover, they primar-

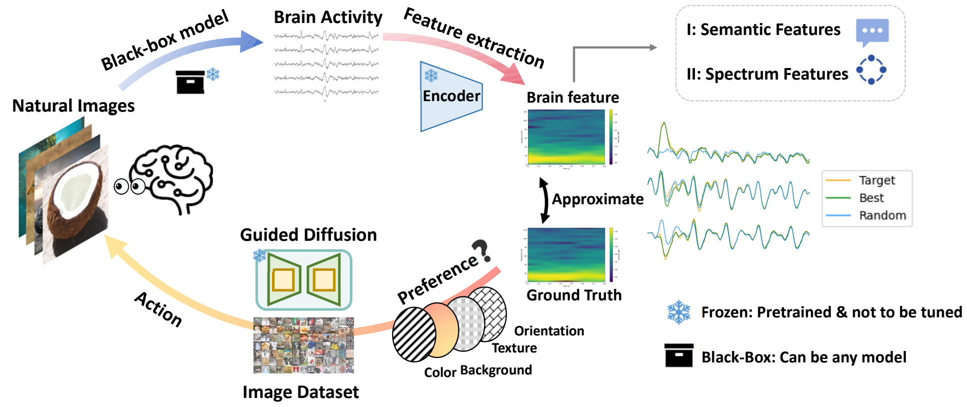

Figure 1: **Conceptualization.** The closed-loop visual stimulation framework includes three core components. (1) The *Black-box model* is used as a surrogate brain to generate neural responses to visual stimulation, and can be replaced by EEG data recorded from human participants in real closed-loop experiments. (2) The *Encoder* extracts the brain features associated with the target neural activity, which can be designed flexibly according to specific control goals. (3) The controllable image generator *Guided diffusion* synthesizes several candidate images. Through closed-loop iteration, the system continuously refines the visual stimulation to achieve the desired brain response.

ily focus on optimizing stimuli for individual neurons, which cannot reflect the complex, distributed neural coding patterns observed at a macroscopic scale, such as those captured in EEG signals. More recently, (Luo et al., 2024b) introduced the Visual Evoked Potential (VEP) Booster, a closed-loop framework designed to generate EEG biomarkers through visual stimulation. However, the VEP Booster primarily generates stroboscopic visual stimuli, rather than natural images that align with the known selectivity principles of the visual system (e.g., preferences for faces, objects, or semantic categories). Therefore, it is crucial for a closed-loop neuromodulation framework that uses natural image stimuli, capable of both flexibly controlling EEG signals and respecting the brain's inherent selectivity.

In this work, we develop a flexible closed-loop visual stimulation framework designed to achieve controllable EEG responses, as illustrated in Figure 1. By leveraging existing natural image datasets (Hebart et al., 2019) and pre-trained image generation models (Rombach et al., 2022), we utilize state-of-the-art diffusion models to identify fine-grained brain functional specializations in a data-driven manner. Our contributions are summarized as follows:

- We introduce a cutting-edge closed-loop visual neurofeedback framework that synthesizes natural images to control brain activity signatures. Our framework establishes a causal mapping between synthetic visual stimuli and specific EEG features in visual regions.
- By replacing traditional human EEG experiments with a black-box model (serving as a surrogate brain to predict neural responses to stimuli), we minimize dataset biases and enhance the model's ability to generalize to novel stimuli, providing valuable insights for future human subject experiments.
- We leverage state-of-the-art diffusion models to identify fine-grained visual selectivity, incorporating natural image priors to improve generalization. It allows for flexible design according to specific control goals, such as image retrieval to approximate neural activity generated by a reference image.

2 RELATED WORK

Mapping Selectivity and Invariance from EEG. Modern neuroscience posits that specific regions of the brain exhibit distinct sensitivities or preferences for particular types of stimuli (Tesileanu et al., 2022). This phenomenon, known as *selectivity*, describes how neurons or neural networks in these regions respond strongly to specific visual inputs. For instance, (Luo et al., 2024a) highlights cases where neurons demonstrate pronounced selectivity for particular stimuli, underscoring their preference for specific visual features. In contrast, *invariance* refers to the brain's ability to respond consistently to distinct stimuli that convey the same information. In other words, different stimuli can elicit similar patterns of brain activity (Baroni et al., 2023). To explore the intrinsic invariance shared by ANNs and the brain, (Feather et al., 2023) proposed a method for generating model-equivalent stimuli, also known as model Metamers. Metamers evoke identical neuronal activations as a reference stimulus, providing a robust framework to examine the internal states of AI models and their alignment with neural processes. This approach provides critical insights into the shared computational principles underlying how artificial and biological systems process and represent information.

Closed-loop Control of Brain Activity. Neuromodulation based on visual stimulation offers potential applications in understanding neural mechanisms and developing treatments for neurological disorders. For instance, 40-Hz light flicker to entrain gamma oscillations in the brain has potential for treating Alzheimer's disease (Iaccarino et al., 2016; Martorell et al., 2019), and depression. Closed-loop control of brain activity using visual stimulation is a promising approach for regulating neural responses through real-time monitoring and feedback. Traditionally, studies in this area have employed cutting-edge algorithms to enhance the efficiency and precision of signal processing and decision-making, thereby advancing the intelligence of closed-loop systems. (Bashivan et al., 2019) applied gradient descent to optimize the characteristics of target neuron excitation or inhibition and used the resulting gradients to update the ANN-based stimulus image generator, effectively regulating the activity of specific target neurons. (Walker et al., 2019) proposed an innovative experimental paradigm called "inception loops", which combines *in vivo* recordings with in silico modeling to synthesize optimal visual stimuli that can stimulate specific neuronal responses. (Luo et al., 2024b) employed a closed-loop strategy wherein a trained generative model to continuously refine the VEP image of the biomarker. This iterative process produced higher-quality EEG data, demonstrating the utility of closed-loop methods in improving biomarker-driven optimization framework. (Pierzchlewicz et al., 2024) introduced a new method for optimizing and generating Most Exciting Inputs (MEIs) through Energy Guidance (EGG) in neurons of the rhesus monkey V4 region.

Brain-conditioned Image generation. Gradient-based brain condition generation is becoming a pivotal technique in optimizing visual stimulus design, particularly for neurofeedback and brain-computer interface (BCI) applications (Luo et al., 2024b;a). This method relies on iteratively refining stimuli by backpropagating the gradients of neural activity representations to steer brain states toward desired conditions or achieve specific cognitive effects. Such an approach enables precise, adaptive stimulus optimization in response to real-time neural feedback, forming the basis for personalized brain modulation.

Recent advances have expanded the scope of gradient-based techniques by integrating more sophisticated neural models and leveraging high-dimensional neural representations captured by EEG, fMRI (Gu et al., 2023), and other brain imaging modalities. These advances have significantly enhanced the precision of stimulus generation, accounting for individual variability in neural responses. Moreover, by incorporating deep learning models, such as guided diffusion models (Ye et al., 2023), researchers can now generate highly detailed and context-specific stimuli tailored to align closely with target neural states, further advancing the field of brain condition generation.

3 METHOD

We aim to find the optimal stimulus image through either image retrieval or editing within a searchable space to produce specific neural activity recorded from EEG. We demonstrate our overall framework in Figure 2. This closed-loop system is adaptable to various control objectives, enabling it to perform retrieval and generation tasks in Figure 2(A). Specifically, we design two distinct feature extractors for retrieval and generation, respectively, and illustrate how our strategy modulates brain activity by controlling the visual stimulus presented in Figure 2(B)(C). If the system tends to prefer images with specific colors or textures, it will recognize the relevance of these features to the target class and assign them higher weight in subsequent iterations. Through this closed-loop iterative process, the system can optimize the visual stimulus to better evoke the desired EEG responses.

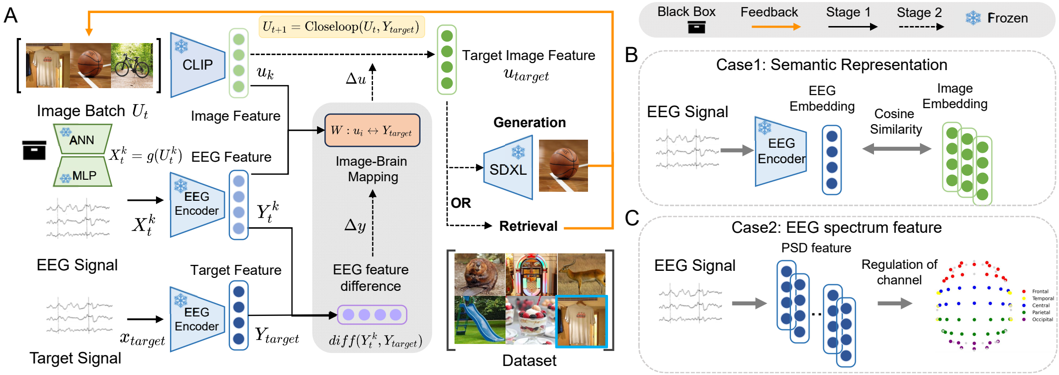

Figure 2: **Closed-loop visual stimulation framework via EEG-based controllable generation.** (A) We employs a closed-loop iterative process to approximate neural representations derived from EEG signals X. The encoding model g, which maps images to synthetic EEG, is designed as a black-box model to broadly simulate the process of regulating brain responses Y. The EEG Encoder f is tailored to accommodate various neural features U. The image with a higher brain similarity score $sim\langle u_j, u_{\text{target}}\rangle$ is retained and passed back to the image generator to generate optimized stimuli with a natural image. (B) Example of semantic feature extraction from a pre-trained EEG encoder f, aligned with CLIP embedding. In this case, our algorithm performs a retrieval task to identify the optimal image u_i that best matches the u_{target}. (C) Channel-wise energy feature using Power Spectral Density (PSD) features. Generative models are iteratively applied to modify the images. For more details, refer to Section 3.1.

3.1 CLOSED-LOOP FRAMEWORK

We formulate the EEG signals as $X \in \mathbb{R}^{C\times T}$, where C is the number of EEG channels and T represents the length of the data points. The image set, containing N images, is denoted as Ω, with each image labeled sequentially with $1, 2, ..., N$ for simplicity. Concurrently, we use the encoding model g to predict brain activity signal $X = g(U) \in \mathbb{R}^{N\times C\times T}$. Our objective is to derive brain activity embeddings $Y = f(g(U)) \in \mathbb{R}^{N\times F}$ from the images $I \in \mathbb{R}^{N\times 3\times H\times W}$, where f is the feature mapping function from X to Y, U is the set of stimulus images set, and F represents the dimension of embedding. Our iteration process can be approximated as a value-based iterative Markov Decision Process (MDP). The state is represented as the probability distribution of each image $P(u)$ in the image database belonging to target category u_{target}. The state updated after each iteration corresponds to a state transition in the MDP. In each iteration, the framework determines which image to select, represented as an action in the MDP. In our model, let $j \in [\![1, N]\!]$, the reward is defined as the similarity score between the selected or generated image u_i from database and the features of the target category u_{target}:

$$sim\langle u_j, u_{\text{target}}\rangle = \frac{f\left(g(u_j)\right) \cdot f\left(g(u_{\text{target}})\right)}{\|f\left(g(u_j)\right)\|\|f\left(g(u_{\text{target}})\right)\|} \tag{1}$$

Let u_i be any image in the search space, which is the target of model evaluation. During the iteration of the t to $t+1$ step, we update $S_{t+1}(u_i)$ based on u_i. The weight coefficient α controls the cumulative probability increment. Let u_+ be the image that the system considers to be closest to the target category by computing EEG feature similarity. For the history subset H of selected images k, the posterior probability that u_i is the most similar to the target image is updated as follows:

$$S_{t+1}(u_i) = \alpha \cdot S_t(u_i) + (1-\alpha) \cdot \frac{\exp\left(s(u_+, u_i)\right)}{\sum_{k=1}^{H} \exp\left(s(u_+^k, u_i)\right)} \cdot S_t(u_i) \tag{2}$$

where s is the cosine similarity of CLIP (Radford et al., 2021) embedding. The update probability $P_{t+1}(u_i)$ for u_i is computed by normalizing the exponentiated value of the updated score $S_{t+1}(u_i)$ over the sum of exponentiated scores for all u_j in the dataset, ensuring that the probabilities across all u_i sum to 1:

$$P_{t+1}(u_i) = \frac{\exp\left(S_{t+1}(u_i)\right)}{\sum_{j=1}^{N} \exp\left(S_{t+1}(u_j)\right)} \tag{3}$$

In step t iteration, our framework operates as follows. First, we initialize a set of random images $U_0 = \{u_1, u_2, \ldots, u_j\}$. Using the pretrained encoding model g to synthesize EEG signals X_i from these stimuli. Second, for any given representation function Y_i, we calculate the neural activity representation $Y_i = f(g(U_i)) \in \mathbb{R}^{N \times F}$ from the predicted signal x_i, to estimate the difference based on the target neural representation Y_{target}. Third, the similarity score $sim\langle u_j, u_{\text{target}} \rangle$ between each neural representation derived from each current stimulus u_j and the target representation is computed. Subsequently, stimulus images exhibiting higher similarity scores are more likely to be selected. Based on $sim\langle u_j, u_{\text{target}} \rangle$, stimulation is probabilistically sampled, favoring images that are closer to the target representation. Finally, the sampled images are used to retrieve similar images for the step $t + 1$ or input into the diffusion model to generate new stimulus samples.

3.2 BLACK-BOX ENCODING MODEL

Instead of collecting real EEG data, we employ an image-computable brain encoder g_θ, treated as a black-box model, to map an image $I_i \in \mathbb{R}^{3 \times H \times W}$ to a synthetic EEG X_i. This synthetic EEG can later be replaced with EEG recordings obtained from human participants in real experiments. Moreover, we assume that our framework remains effective regardless of the specific structure of the encoding model, allowing us to focus on the advancements of the framework itself rather than the details of the encoding model's architecture. To ensure robustness, we use two different CNN models, AlexNet (Krizhevsky, 2014) and CORnet-S (Kubilius et al., 2019), as feature extractors and train regressors to predict the ground truth of EEG $\hat{X}$.

In the encoding model, we modify the CNN's 1000-neuron output layer to a $C \times T$-neuron layer, where each neuron corresponds to one of the flattened EEG data ponits $C \times T$. Each subject is assigned to unique model parameters, achieved by pretrained models and across all EEG time points T. Given the input training images I and the corresponding target EEG data $\hat{X}$, the model updates its weights by minimizing the mean squared error (MSE) between predicted EEG X and the $\hat{X}$. This setup ensures a personalized and accurate prediction of synthetic neural activity.

3.3 INTERACTIVE SEARCH

To find the optimal stimulus that causes the target neural activity, we search for images that produce EEG feature similar to target. The target query image is assumed to be unknown, but the target EEG feature is observable. In this experiment, we set the transition probability as the global cumulative probability and then sample new image stimuli in each step using a roulette wheel method. To address the challenge of initiating retrieval without a clear query image, we use the mathematical framework of (Ferecatu & Geman, 2007), based on mind matching. This approach begins with a random sample of images, and through iterative steps, the user selects the image that most closely aligns with the category in their mind. In our retrieval case, this process is adapted to match target neural feature. The detailed algorithmic procedure is presented in Algorithm 1. This algorithm can effectively find an optimal subset of images that maximizes the similarity score with respect to the target EEG feature.

In our framework, the *Closed-loop Retrieval Iteration Algorithm* operates as a sequence of state transitions aimed at maximizing the similarity between current neural feature and the target. The process begins with a randomly selected set of images U_0, without any prior knowledge of the specific features of the target image. We use a roulette wheel algorithm to select from current images according to $sim\langle u_j, u_{\text{target}} \rangle$. The system updates the probability $p_t(u_j)$ of each image in the database belonging to the target class based on the response model's prediction $Y = f(g(U)) \in \mathbb{R}^{N \times F}$. Subsequently, the system calculates the distance between the brain activity feature vector of the target image and the brain activity feature vector predicted by the image selected by the roulette wheel algorithm (i.e., the image that is considered to be closer to the target class). Once an image is optimal in a round, the likelihood of similar images in the search space belonging to the target class increases. See Appendix A.1.1 for more implementation details.

3.4 HEURISTIC GENERATION

Retrieving the optimal image stimulus only in the image feature space limits the potential to get closer to the target brain activity. To design an optimal stimulus to the greatest extent, we use

Algorithm 1 Closed-loop Retrieval Iteration Algorithm

```
1: Initialize: Set initial set $U_0 = \{u_1, u_2, \ldots, u_k\}$, where $U_0 \subseteq \Omega$.
2: repeat
3:     Action Selection: $U_t = \{u_1, u_2, \ldots, u_k\}$ from $\Omega$ based on $p_t(u)$.
4:     Reward Calculation:
           $$sim_{\max} = \max\ sim\langle u_k, u_{\text{target}}\rangle$$
5:     if $sim_{\max} < threshold_1$:
6:         Go to Step 3.
7:     else:
8:         Optimal Action Reference:
           $$\{u_{\text{top1}}, u_{\text{top2}}\} = \arg \max_{\substack{u_k \in U_t \\ \text{top 2}}} \frac{\exp\left(sim\langle u_k, u_{\text{target}}\rangle\right)}{\sum_{u_h \in H} \exp\left(sim\langle u_h, u_{\text{target}}\rangle\right) + \sum_{u_k \in U_t} \exp\left(sim\langle u_k, u_{\text{target}}\rangle\right)}$$
9:         if $sim\langle u_{target}, u_{top1}\rangle$ or $sim\langle u_{target}, u_{top2}\rangle > threshold_2$:
10:            CLIP-based Retrieval: Using $u_{\text{top1}}$ and $u_{\text{top2}}$, retrieve the top-$k$ images $\{u'_1, u'_2, \ldots, u'_k\}$ from $\Omega$ that have the highest similarity $s$:
               $$u'_k = \arg\max_{u \in U} \{s(u, u_{\text{top1}}), s(u, u_{\text{top2}})\}.$$
11:            Update Action Set: Update the subset $U_{t+1}$:
               $$U_{t+1} = \{u'_1, u'_2, \ldots, u'_k\}.$$
12:            Recurse on $U_{i+1}$: Repeat the process for the new action set $U_{t+1}$, treating it as the current action set $U_t$ for the next iteration.
13: until $s_{\max} \geq threshold_{primary}$
14: Return: Return the best action set $U_t$ as the final set of retrieved images.
```

StableDiffusion XL-turbo for image-guided optimal stimulus generation. The pretrained guided diffusion model $G(U_t)$ generates new visual stimuli via image-to-image. Based on MDP, we use a genetic algorithm to assist the generator in generating image in the direction of the target neural activity while ensuring global optimality. Our specific algorithm process is shown in Algorithm 2. Unlike Algorithm 1, after sampling the stimulus image in each step of roulette, we partially cross the image features, and randomly sample new image samples from the image space. Mutation is performed based on the current images features U_t. See Appendix A.1.2 for more details. In the process of evolution, the relative order of original CLIP features retained by per sample to ensure that normal semantic images that are understandable to humans can still be generated after mutation.

4 EXPERIMENTS

4.1 SETUP

Datasets We conducted our experiments using the training set of the THINGS-EEG2 dataset (Gifford et al., 2022; Grootswagers et al., 2022), which consists of a large EEG corpus from 10 human subjects performing a visual task. The experiments used the Rapid Serial Visual Presentation (RSVP) paradigm for orthogonal target detection tasks to ensure participants' attention to the visual stimuli. All 10 participants underwent 4 equivalent experiments, resulting in 10 datasets with 16,540 unique training image conditions, each repeated 4 times, and 200 unique testing image conditions, each repeated 80 times. In total, this yielded (16,540 training image conditions × 4 repetitions) + (200 testing image conditions × 80 repetitions) = 82,160 image trials. The original data were recorded using a 64-channel EEG system with a 1000 Hz sampling rate. For preprocessing, the data were first downsampled to 250 Hz and 17 channels were selected from the occipital and parietal regions, which are closely related to the visual system. The EEG data were then segmented into trials, spanning from 0 to 1000 ms post-stimulus onset, with baseline correction applied using the mean of the 200 ms pre-stimulus period. Multivariate noise normalization was applied to the training data (Guggenmos et al., 2018).

Algorithm 2 Closed-loop Generative Iteration Algorithm

```
Initialize: Set initial set $U_0 = \{u_1, u_2, \ldots, u_k\}$, where $U_0 \subseteq \Omega$.
repeat
    Selection: $U_t = \{u_1, u_2, \ldots, u_k\}$ from $\Omega$ based on $p_t(u)$.
    Sampling: Based on the calculated similarity scores, sample from $U_t$ using:
        $$P(u_k) = \frac{\exp\left(sim\langle u_k, u_{\text{target}}\rangle\right)}{\sum_{u_{k'} \in U_t} \exp\left(sim\langle u_{k'}, u_{\text{target}}\rangle\right)}$$
    where $P(u_k)$ is the sampling probability for each $u_k \in U_t$.
    Crossover: Draw two distinct samples $u_a, u_b$ from $U_t$ based on $P(u_k)$, and output new samples by combining the partial embedding of $u_a$ and $u_b$:
        $$F(u^{(1)}_{\text{tmp}}) \leftarrow \alpha \cdot F(u_a) + (1 - \alpha) \cdot F(u_b)$$
        $$F(u^{(2)}_{\text{tmp}}) \leftarrow \alpha \cdot F(u_b) + (1 - \alpha) \cdot F(u_a)$$
    where $\alpha$ is a crossover control factor.
    Mutation: Based on $P(u_k)$, apply mutation to the drawn images $u_{\text{c}}$ from $U_t$, and another image $u_{\text{d}}$ is drawn from the remaining $U_t$ (i.e., $U_t \setminus \{u_{\text{c}}\}$):
        $$F(u^{(3)}_{\text{tmp}}) \leftarrow \beta \cdot F(u_c) + (1 - \beta) \cdot F(u_d)$$
    where $\beta$ is a mutation control factor.
    Generation: Generate a new set of images $U_{\text{gen}} = \{u^{(1)}_{\text{gen}}, u^{(2)}_{\text{gen}}, u^{(3)}_{\text{gen}}\}$ according to the outputs of crossover and mutation phase.
    Selection: Combine $U_{\text{gen}}$ with $U_t$ and randomly selected samples $U_{\text{random}} = \{u^{(1)}_{\text{ran}}, u_{\text{ran}^{(2)}}, \ldots, u^{(n)}_{\text{ran}}\}$, where $U_0 \subseteq \Omega$.
    Update Action Set: Update the subset $U_{t+1}$:
        $$U_{t+1} \leftarrow \{U_t, U_{\text{gen}}, U_{\text{random}}\}$$
    Replace the old population with the new set of images $U_{i+1}$.
until similarity score converges or reach the maximum number of cycles.
```

Encoding Model In the training phase, we used a batch size of 64 images and the Adam optimizer with a learning rate of 10^{-5}, a weight decay term of 0, and default values for other hyperparameters. Training was conducted over 50 epochs, with EEG responses for test image conditions synthesized using the model weights from the epoch that yielded the lowest validation loss. For each participant, the models generated EEG signals with a shape of 17 EEG channels $\times$ 250 EEG time points as the output corresponding to the input images. All experiments can be done on a single NVIDIA 4090 GPU.

Target Features of EEG We designed different target EEG features for different cases. In the retrieval task based on semantic representation, system randomly selects images with an index greater than 12 in each class of the test set of the THINGS-EEG2 as target images, where these images are excluded from the retrieval space of $200 \times 12 = 2400$ images. In the generation task based on spectral features, in order to ensure that the regulation is meaningful, we calculated the EEG feature similarity matrix corresponding to the prediction of the 200×1 image from the test set, and took the top-3 images with the lowest similarity in each class after row averaging as the target for testing. We use the pre-trained encoding model (AlexNet, CORnet-S) and pre-trained EEG encoder (ATM-S (Li et al., 2024), PSD) to process the target images and get their corresponding EEG features.

4.2 REGULATION OF BRAIN SEMANTIC REPRESENTATION

In order to verify the effectiveness of our EEG-based closed-loop visual stimulation framework for achieving the target neural activity representation, we first conducted a retrieval task in the image space. We regarded the encoding model g as a black-box model to ensure that the gradient is not used to update the parameters of the encoding model, so as to better focus on the closed-loop regulation

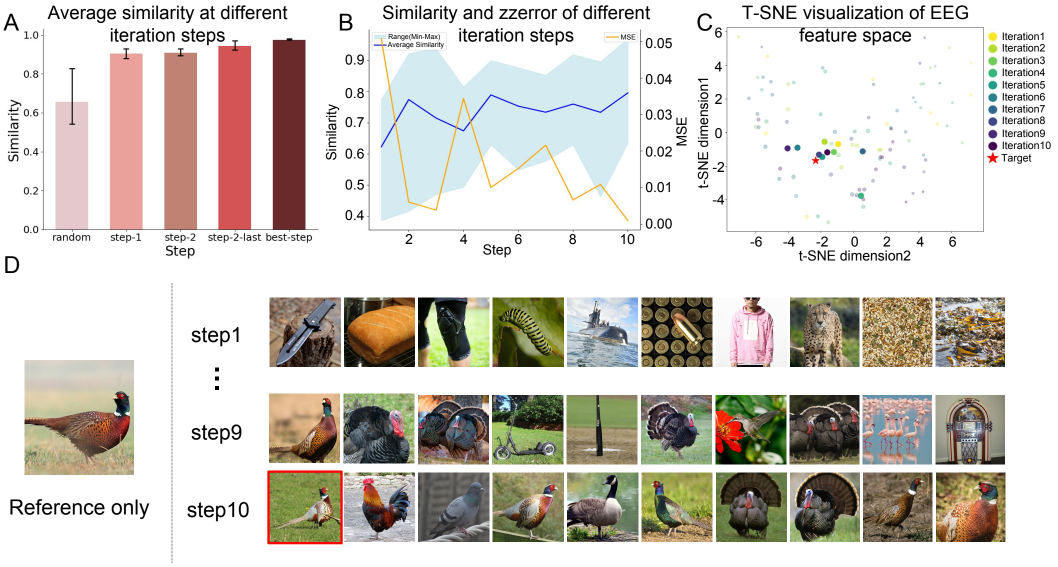

Figure 3: **Results of our framework in the retrieval task.** (A) Similarity between the neural representation obtained by our framework at different iteration steps (i.e., step-1, step-2, step-2-last, best-step) and the target neural representation compared to random stimulus (i.e., random). (B) The evolution of EEG representation similarity (blue) and loss curves (yellow) on Subject 8 at different iteration steps. (C) The t-SNE visualization of Subject 8's latent trajectories within the feature space across all iterations. (D) The images retrieved by our framework at different iteration steps. Only the neural activity representation evoked by the reference image is known during the iteration process.

framework itself. We performed the retrieval task in the test set of THINGS-EEG2 dataset with $200 \times 12 = 2400$ images. We use the EEG encoder ATM-S to obtain EEG semantic representations aligned with 1×1024 CLIP image features. Before the retrieval begins, random initialization ensures 10 initial points are scattered as much as possible in the image feature space. During the search process, each initial image sample calculates the cosine similarity with the global image features, and uses the cumulative probability to have more reasonable opportunities to select image samples that can produce new and closer to the target EEG neural representation. In the image feature space, through the initial initial image sample point, it continuously expands to form a small area and iterates, and finally approaches the theoretically optimal stimulus image sample. The condition for the iteration to terminate is similarity $s(u_+, u_i) > 0.97$.

Based on semantic representation, our retrieval results are shown in Figure 3. In Figure 3(A), we plotted the similarity scores of stimuli and random stimuli at different time steps of the iteration process. Figure 3(B) shows the average similarity and mean square error with the expected EEG features at different iteration time steps for subject 8. Figure 3(C) illustrates the convergence patterns from initial to final positions for selected iterations (e.g., iterations 1 and 10) over multiple cycles. In each iteration, ten images are viewed, with points representing the closest match to the target stimulus at each step. Notably, these points show a gradual approach toward the target stimulus, marked by a red pentagram, across successive iterations. For a given target neural activity representation, our framework iteratively predicts intermediate EEG results and retrieves stimulus images at each iteration. Notably, only the neural activity representation evoked by the reference image is known throughout this process. Through successive iterations in 3(D), the framework refines its selection, ultimately retrieving an image (outlined in red) that closely matches the semantic representation of the reference image.

4.3 REGULATION OF INTENSITY OF NEURAL ACTIVITY

We implemented a closed-loop stimulus image generation framework using the $200 \times 1 = 200$ image space of THINGS-EEG2 as initialization. We set the crossover rate α to 0.6, the mutation rate β to 0.2, and randomly select 10 images from 200 images during initialization. We used StableDiffusion

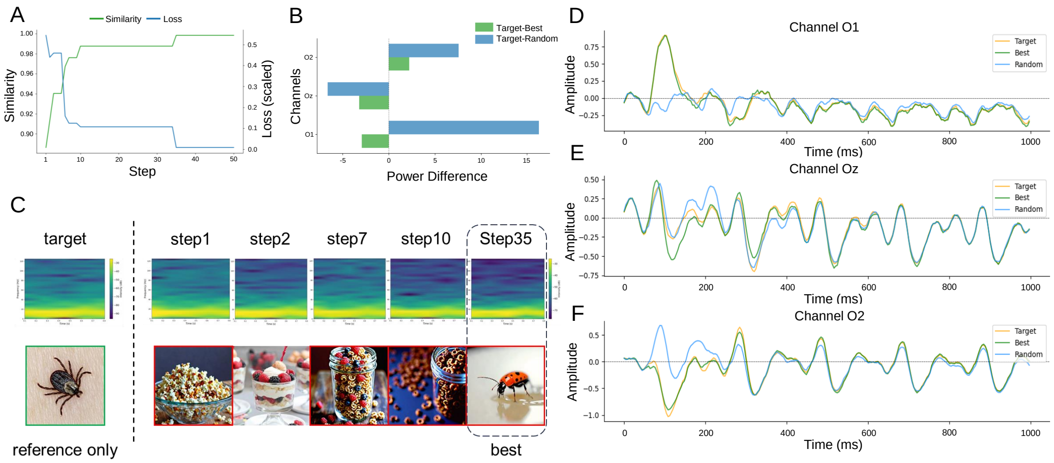

Figure 4: **Results of our framework in the generation task.** (A) Similarity and loss curves of EEG neural representations for Subject 8. (B) The difference of PSD between the neural activity representations evoked by the final step of generated and random stimulus, with the target neural representations used as the relative baseline. (C) For a given target EEG semantic representation, our framework iteratively predicts synthetic data, extract feature and synthesizes images at each iteration. The image enclosed by a red border represents the image synthesized by the generator, while the unbordered image is a sample selected from the original dataset. (D) EEG timing diagram generated by our stimulus images for O_1 channel. (E) EEG timing diagram generated by our stimulus images for O_z channel. (F) EEG timing diagram generated by our stimulus images for O_2 channel.

XL-turbo (Rombach et al., 2022) integrated by IP-Adapter (Ye et al., 2023) to generate new samples each time based on the new stimulus images obtained after crossover and mutation, and randomly selected 2 samples from the image feature space, calculated the similarity of EEG activity representation, and selected the next step of stimulation according to the roulette method of cumulative probability.

The results of our stimulus generation experiments are shown in Figure 4. Figure 4(A) shows the similarity and mean square error between the EEG features generated by the step stimulation image at different iterations and the target EEG features. In addition, we calculated the explained variance of different channels and selected the three channels O_1, O_z, and O_2 with the largest variance for regulation. Figure 4(B) shows the comparison of the PSD of the EEG predicted by the random and step-best samples relative to the target EEG representation. Figure 4(DEF) plots the synthetic EEG of three different channels obtained by step-best, random and target stimulation images respectively. All three channels show that the EEG corresponding to step-best, random and target images is quite different before 100 data points (corresponding to 0.4s). After 0.4s, due to the limitations of the encoding model itself, the synthetic EEG of the target image is not much different from the synthetic EEG of the optimal stimulation and the synthetic EEG of the random image. This corresponds to Fig.4 in (Gifford et al., 2022). Using the tick image as an example, Figure 4(C) shows the image and its corresponding time-frequency features, as well as the generated image and corresponding features at each iteration.

4.4 REGULATION OF INDIVIDUAL VARIABILITY

Table 1 summarizes the results in the retrieval setting (corresponding to the representation score, SS) and the generation model setting (corresponding to the intensity score, IS), highlighting the results of our framework in achieving the optimal number of iterations in a given search space. The data show that for different target EEG features, our method has a good improvement in feature similarity across different subjects. For instance, the similarity score (SS) of the semantic feature of Subject 7 is improved from 0.874 in step-1 to 0.974, with an improvement of 10.04%. Similarly, the feature similarity score (IS) of the channel intensity of Subject 8 is improved from 0.913 in step-1 to 0.990, accompanied by a 7.744% improvement. Even on the subjects with poor performance, our framework achieves a positive performance, which shows that our framework has a generalized improvement effect across different subjects, highlighting its potential in practical applications.

Table 1: **Performance (EEG semantic representation and intensity) of brain responses.** We provide two metrics: EEG semantic representation score (i.e., SS) and EEG response intensity score (i.e., IS) to measure the difference between the neural activity generated by the optimal stimulation image we obtained and the target EEG neural activity.

	Step-1		Step-Best		Improvement	
Subject	SS	IS	SS	IS	ΔSS (%)	ΔIS (%)
1	0.871	0.989	0.967	0.997	9.593	0.801
7	0.874	0.960	0.974	0.995	10.040	3.444
8	0.904	0.913	0.976	0.990	7.162	7.744
10	0.915	0.986	0.961	0.998	4.587	1.163

5 DISCUSSION AND CONCLUSION

In this study, we developed a flexible closed-loop visual stimulation framework for controlling EEG signatures. To the best of our knowledge, this is the first work to successfully employ closed-loop generation of natural images to modulate brain activity.

Technical Impact: Our framework demonstrated the potential of flexibly controlling EEG signals through visual stimulation. We employed a closed-loop iterative strategy, where new random stimuli are sampled each time a new round of stimulus images is generated. The gradient of the EEG objective is passed to the diffusion model in a proxy manner, eliminating the need for training or updating the weights of the generative model. This approach demonstrates that our framework is an efficient and optimal closed-loop stimulus generation method, capable of achieving the desired neural modulation without requiring any model parameter updates. It opens new avenues for applications in brain-computer interfaces, neurofeedback systems, and therapeutic interventions for neurological disorders that require precise regulation of brain activity (Jang et al., 2021; Alamia et al., 2023).

Neuroscience Insights: Our study provides valuable insights into the neural mechanisms underlying visual perception and stimulus processing. First, we demonstrated the successful modulation of activity in specific electrode channels, indicating that neural activity in targeted brain regions can be fine-tuned through controlled visual stimulation. Second, we showcased our framework's ability to guide the brain in generating specific neural representations, which is crucial for understanding how different brain regions process visual information and respond to external stimuli. Furthermore, our framework establishes a causal link between visual stimuli and neural responses. By connecting specific EEG patterns to visual representations, our work deepens the understanding of how neural signatures correlate with perceptual experiences.

Interesting Phenomena and Future Directions: Our findings demonstrate that different stimulus images in our framework can produce similar or identical EEG features, confirming the existence of Metamers (Feather et al., 2023) and suggesting that Metamers are not necessarily unique. The presence of multiple Metamers highlights the ill-posed nature of generating visual stimuli conditioned on EEG features. Future research should focus on understanding the neural mechanisms that lead to the generation of similar EEG features from different stimuli. Another promising direction is the integration of more sophisticated models that account for inter-individual variability in neural responses, aiming to fine-tune the stimulus generation process for personalized neuromodulation and enhanced brain-computer interaction (Alamia et al., 2021). Further exploration could involve integrating this closed-loop framework with other brain imaging modalities, such as fMRI or MEG. Additionally, it is important to test various control goals aimed at regulating specific EEG characteristics to modulate brain functions, such as a control objective on EEG features for emotion regulation.

REFERENCES

Andrea Alamia, Milad Mozafari, Bhavin Choksi, and Rufin VanRullen. On the role of feedback in visual processing: a predictive coding perspective. *arXiv preprint arXiv:2106.04225*, 2021.

Andrea Alamia, Milad Mozafari, Bhavin Choksi, and Rufin VanRullen. On the role of feedback in image recognition under noise and adversarial attacks: A predictive coding perspective. *Neural Networks*, 157:280–287, 2023.

Luca Baroni, Mohammad Bashiri, Konstantin F Willeke, Ján Antolík, and Fabian H Sinz. Learning invariance manifolds of visual sensory neurons. In *NeurIPS Workshop on Symmetry and Geometry in Neural Representations*, pp. 301–326. PMLR, 2023.

Pouya Bashivan, Kohitij Kar, and James J DiCarlo. Neural population control via deep image synthesis. *Science*, 364(6439):eaav9436, 2019.

Dave Epstein, Allan Jabri, Ben Poole, Alexei Efros, and Aleksander Holynski. Diffusion self-guidance for controllable image generation. *Advances in Neural Information Processing Systems*, 36:16222–16239, 2023.

Russell Epstein and Nancy Kanwisher. A cortical representation of the local visual environment. *Nature*, 392(6676):598–601, 1998.

Jenelle Feather, Guillaume Leclerc, Aleksander Madry, and Josh H McDermott. Model metamers reveal divergent invariances between biological and artificial neural networks. *Nature Neuroscience*, 26(11):2017–2034, 2023.

Marin Ferecatu and Donald Geman. Interactive search for image categories by mental matching. In *2007 IEEE 11th International Conference on Computer Vision*, pp. 1–8. IEEE, 2007.

Alessandro T Gifford, Kshitij Dwivedi, Gemma Roig, and Radoslaw M Cichy. A large and rich eeg dataset for modeling human visual object recognition. *NeuroImage*, 264:119754, 2022.

Tijl Grootswagers, Ivy Zhou, Amanda K Robinson, Martin N Hebart, and Thomas A Carlson. Human eeg recordings for 1,854 concepts presented in rapid serial visual presentation streams. *Scientific Data*, 9(1):3, 2022.

Zijin Gu, Keith Jamison, Mert R Sabuncu, and Amy Kuceyeski. Modulating human brain responses via optimal natural image selection and synthetic image generation. *ArXiv*, 2023.

Matthias Guggenmos, Philipp Sterzer, and Radoslaw Martin Cichy. Multivariate pattern analysis for meg: A comparison of dissimilarity measures. *Neuroimage*, 173:434–447, 2018.

Martin N Hebart, Adam H Dickter, Alexis Kidder, Wan Y Kwok, Anna Corriveau, Caitlin Van Wicklin, and Chris I Baker. Things: A database of 1,854 object concepts and more than 26,000 naturalistic object images. *PloS one*, 14(10):e0223792, 2019.

Hannah F Iaccarino, Annabelle C Singer, Anthony J Martorell, Andrii Rudenko, Fan Gao, Tyler Z Gillingham, Hansruedi Mathys, Jinsoo Seo, Oleg Kritskiy, Fatema Abdurrob, et al. Gamma frequency entrainment attenuates amyloid load and modifies microglia. *Nature*, 540(7632):230–235, 2016.

Hojin Jang, Devin McCormack, and Frank Tong. Noise-trained deep neural networks effectively predict human vision and its neural responses to challenging images. *PLoS biology*, 19(12): e3001418, 2021.

Alex Krizhevsky. One weird trick for parallelizing convolutional neural networks. *arXiv preprint arXiv:1404.5997*, 2014.

Jonas Kubilius, Martin Schrimpf, Kohitij Kar, Rishi Rajalingham, Ha Hong, Najib Majaj, Elias Issa, Pouya Bashivan, Jonathan Prescott-Roy, Kailyn Schmidt, et al. Brain-like object recognition with high-performing shallow recurrent anns. *Advances in neural information processing systems*, 32, 2019.

Bowen Li, Xiaojuan Qi, Thomas Lukasiewicz, and Philip Torr. Controllable text-to-image generation. *Advances in neural information processing systems*, 32, 2019.

Dongyang Li, Chen Wei, Shiying Li, Jiachen Zou, and Quanying Liu. Visual decoding and reconstruction via eeg embeddings with guided diffusion. *arXiv preprint arXiv:2403.07721*, 2024.

Andrew Luo, Maggie Henderson, Leila Wehbe, and Michael Tarr. Brain diffusion for visual exploration: Cortical discovery using large scale generative models. *Advances in Neural Information Processing Systems*, 36, 2024a.

Junwen Luo, Chengyong Jiang, Qingyuan Chen, Dongqi Han, Yansen Wang, Biao Yan, Dongsheng Li, and Jiayi Zhang. The vep booster: A closed-loop ai system for visual eeg biomarker auto-generation. *arXiv preprint arXiv:2407.15167*, 2024b.

Anthony J Martorell, Abigail L Paulson, Ho-Jun Suk, Fatema Abdurrob, Gabrielle T Drummond, Webster Guan, Jennie Z Young, David Nam-Woo Kim, Oleg Kritskiy, Scarlett J Barker, et al. Multi-sensory gamma stimulation ameliorates alzheimer's-associated pathology and improves cognition. *Cell*, 177(2):256–271, 2019.

Pawel Pierzchlewicz, Konstantin Willeke, Arne Nix, Pavithra Elumalai, Kelli Restivo, Tori Shinn, Cate Nealley, Gabrielle Rodriguez, Saumil Patel, Katrin Franke, et al. Energy guided diffusion for generating neurally exciting images. *Advances in Neural Information Processing Systems*, 36, 2024.

Carlos R Ponce, Will Xiao, Peter F Schade, Till S Hartmann, Gabriel Kreiman, and Margaret S Livingstone. Evolving images for visual neurons using a deep generative network reveals coding principles and neuronal preferences. *Cell*, 177(4):999–1009, 2019.

Yongrong Qiu, David A Klindt, Klaudia P Szatko, Dominic Gonschorek, Larissa Hoefling, Timm Schubert, Laura Busse, Matthias Bethge, and Thomas Euler. Efficient coding of natural scenes improves neural system identification. *PLoS computational biology*, 19(4):e1011037, 2023.

Alec Radford, Jong Wook Kim, Chris Hallacy, Aditya Ramesh, Gabriel Goh, Sandhini Agarwal, Girish Sastry, Amanda Askell, Pamela Mishkin, Jack Clark, et al. Learning transferable visual models from natural language supervision. In *International conference on machine learning*, pp. 8748–8763. PMLR, 2021.

Robin Rombach, Andreas Blattmann, Dominik Lorenz, Patrick Esser, and Björn Ommer. High-resolution image synthesis with latent diffusion models. In *Proceedings of the IEEE/CVF conference on computer vision and pattern recognition*, pp. 10684–10695, 2022.

Tiberiu Tesileanu, Eugenio Piasini, and Vijay Balasubramanian. Efficient processing of natural scenes in visual cortex. *Frontiers in Cellular Neuroscience*, 16:1006703, 2022.

Edgar Y Walker, Fabian H Sinz, Erick Cobos, Taliah Muhammad, Emmanouil Froudarakis, Paul G Fahey, Alexander S Ecker, Jacob Reimer, Xaq Pitkow, and Andreas S Tolias. Inception loops discover what excites neurons most using deep predictive models. *Nature neuroscience*, 22(12): 2060–2065, 2019.

Chen Wei, Jiachen Zou, Dietmar Heinke, and Quanying Liu. Cocog: Controllable visual stimuli generation based on human concept representations. *International Joint Conference on Artificial Intelligence*, 2024.

Hu Ye, Jun Zhang, Sibo Liu, Xiao Han, and Wei Yang. Ip-adapter: Text compatible image prompt adapter for text-to-image diffusion models. *arXiv preprint arXiv:2308.06721*, 2023.

A APPENDIX

A.1 MORE IMPLEMENTATION DETAILS

A.1.1 RETRIEVAL PIPELINE

We provide a more detailed description of algorithm 1. The algorithm begins by initializing equal selection probabilities for each image in the candidate set, denoted as $p_0(u) = \frac{1}{N}$, where N is the total number of images in the retrieval set. This initialization with equal probabilities reflects the absence of prior information, serving as an exploratory phase. In each iteration (representing a **state** in the MDP framework), a subset of images $U_t = \{u_1, u_2, \ldots, u_j\}$ is selected from the candidate images set U based on the current selection probabilities $p_t(u)$.

For each image u_j in the subset U_t the algorithm computes a similarity score $sim\langle u_j, u_{\text{target}}\rangle$ by comparing the image's representation with the target. This similarity score acts as an immediate **reward** within the MDP framework. The maximum similarity score among the subset is identified as a measure of the effectiveness of the current action. If $sim_{\max}$ does not meet a predefined $threshold_1$, the reward is considered insufficient, and the algorithm returns to the image selection step, effectively trying a new action within the same state. If $sim_{\max}$ meets or exceeds the threshold, the algorithm proceeds to identify the two images u_{top1} and u_{top2} with the highest similarity scores. These two images act as reference points for updating the probabilities of other images in the subsequent state.

As for each image u_j in U that surpasses $threshold_2$ with either u_{top1} or u_{top2}, its selection probability $P_{t+1}(u_j)$ is updated by multiplying with a constant factor, representing a policy improvement step that prioritizes images likely to yield higher rewards. After updating, a Softmax function is applied to normalize the probabilities, focusing selection weight on images more similar to the target. This normalization step reflects the transition to a new state with an updated policy. The iteration continues, with the algorithm transitioning through states by selecting new subsets based on the refined probabilities, until $sim_{\max}$ reaches $threshold_{primary}$. At this point, the loop terminates, as the algorithm has successfully identified an optimal subset of images that maximizes the similarity reward to the target.

A.1.2 GENERATION PIPELINE

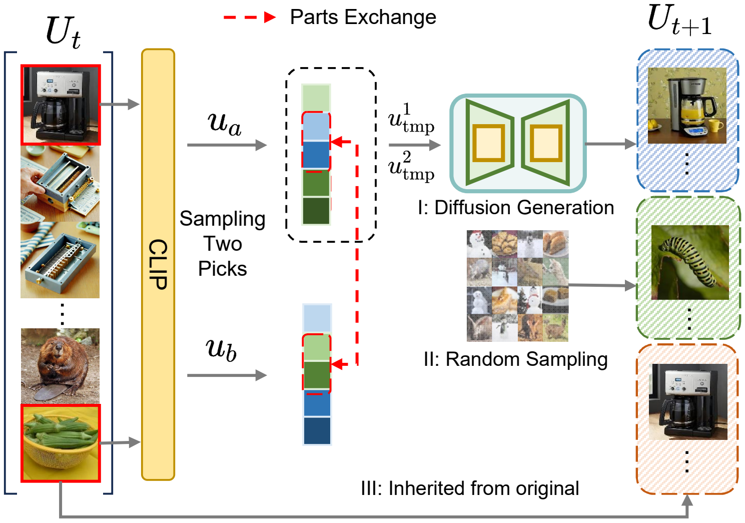

Figure A.1: Generating subsequent images based on the current round is achieved through crossover, variation, and a guided diffusion model. Both crossover and mutation operations preserve the relative ordering of CLIP features, thereby maintaining their semantic coherence.

A.2 ADDITIONAL QUANTITATIVE RESULTS

A.2.1 ITERATION IMPROVEMENT FROM DIFFERENT SUBJECTS

Based on the conclusions drawn from Figure A.4, we employ the pre-trained AlexNet end-to-end model as the EEG encoder and use ATM-S, which is based on S-S (with both the training and testing sets consisting of synthesized signals), to obtain semantic representations aligned with 1×1024 CLIP image features. The experimental design involves randomly selecting 50 categories, resulting in a retrieval space of $50 \times 12 = 600$ images.

For the semantic feature case, we present the iterative performance improvements for three different targets randomly selected from the test set, with results reported for Subjects 1, 7, 8, and 10. As shown in Figure A.2, we calculate the EEG feature similarity of Subject 1, 7, 8, and 10 at random, step-1, and step-best in the iterative process respectively.

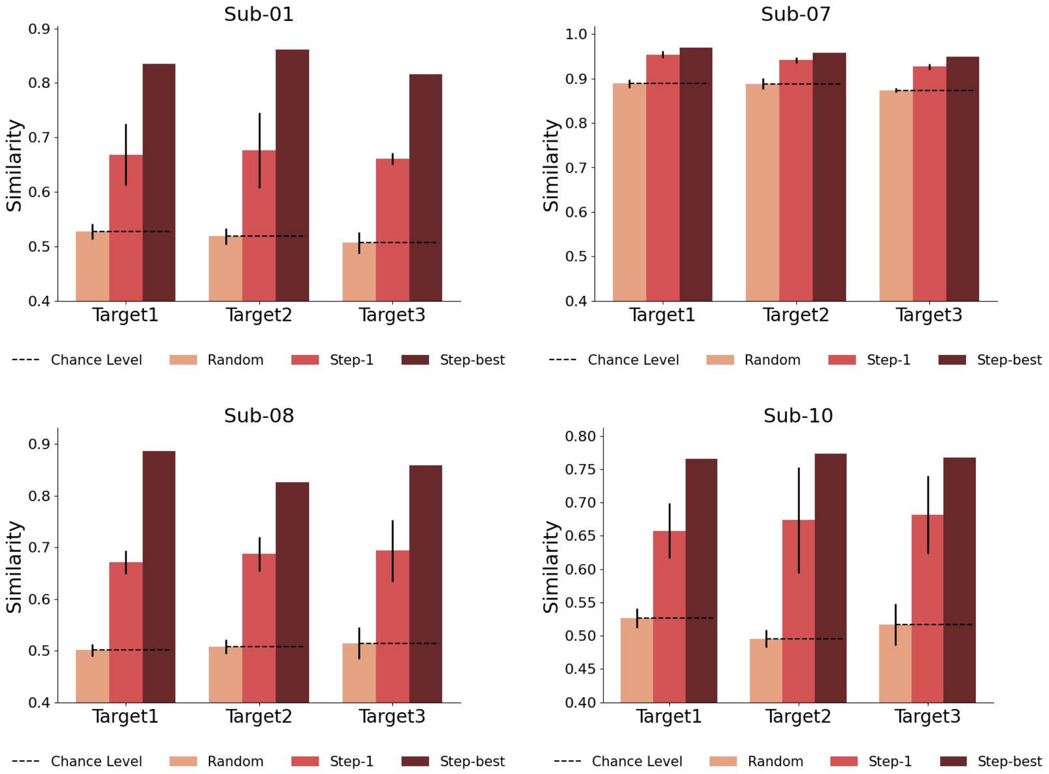

Figure A.2: **Comparison of improved performance by different targets.** We present the similarity scores of EEG features generated by random stimulation, open-loop stimulation (step 1), and step-best stimulation, in comparison to the target features. Each subject randomly selected 3 images from the retrieval space as target images.

A.2.2 PERFORMANCE OF DIFFERENT TARGET IMAGES ACROSS SUBJECTS

We report the results of iterative optimization using different targets in two different cases. The results for each subject are shown, along with the average percentage improvement across 5 random seeds. For the semantic feature case, unlike the setting in Table 1 of the main text, which uses real EEG for training and performs retrieval on synthetic EEG, we determined that training and testing with synthetic EEG yielded the highest accuracy based on the retrieval performance shown in Figure A.4. As a result, we retrained each subject and summarized the results in Table A.1. For the spectral feature case, we selected 3 images using the method described in Section 4, averaged the results across 5 random seeds for each image, and supplemented the iterative improvement performance. Additionally, we performed t-tests on EEG semantic and spectral features across all subjects to assess the efficacy of our proposed method, we also performed correlation analyses to investigate the relationships between semantic features and clip representation, as well as between spectral features (PSD) and clip representation, as shown in Figure A.3.

Table A.1: **Performance (EEG semantic representation and intensity) of brain responses.** We provide two metrics: EEG semantic representation score (i.e., SS) and EEG response intensity score (i.e., IS) to quantify the similarity of generated EEG and target EEG. The table below records the SS & IS values for each subject, showing the SS & IS value from the first round of stimulation, the SS & IS value achieved after multiple rounds of closed-loop control (the optimal result), and the improvement in control. All these results are calculated from pretrained AlexNet models.

	Random		Step-1		Step-Best		Improvement	
Subject	SS	IS	SS	IS	SS	IS	ΔSS (%)	ΔIS (%)
1	0.5174	0.9632	0.6686	0.9729	0.8375	0.9976	16.8859	2.4790
2	0.5197	0.9678	0.6675	0.9764	0.7372	0.9998	6.9701	2.3406
3	0.5113	0.9883	0.6597	0.9927	0.7871	0.9980	12.7402	0.5306
4	0.5065	0.9650	0.6498	0.9836	0.8299	0.9963	**18.0136**	1.2690
5	0.5315	0.9788	0.6937	0.9768	0.8418	0.9979	14.8151	2.1055
6	0.6747	0.9836	0.8099	0.9856	0.8826	0.9961	7.2634	1.0461
7	0.8838	0.8955	0.9410	0.9033	0.950	0.9742	1.8237	**7.0879**
8	0.5077	0.8344	0.6838	0.9435	0.8568	0.9925	17.3066	4.8947
9	0.8465	0.9602	0.9251	0.9751	0.9597	0.9997	3.4662	2.4597
10	0.5128	0.8172	0.6707	0.9705	0.7687	0.9934	9.8032	2.2849

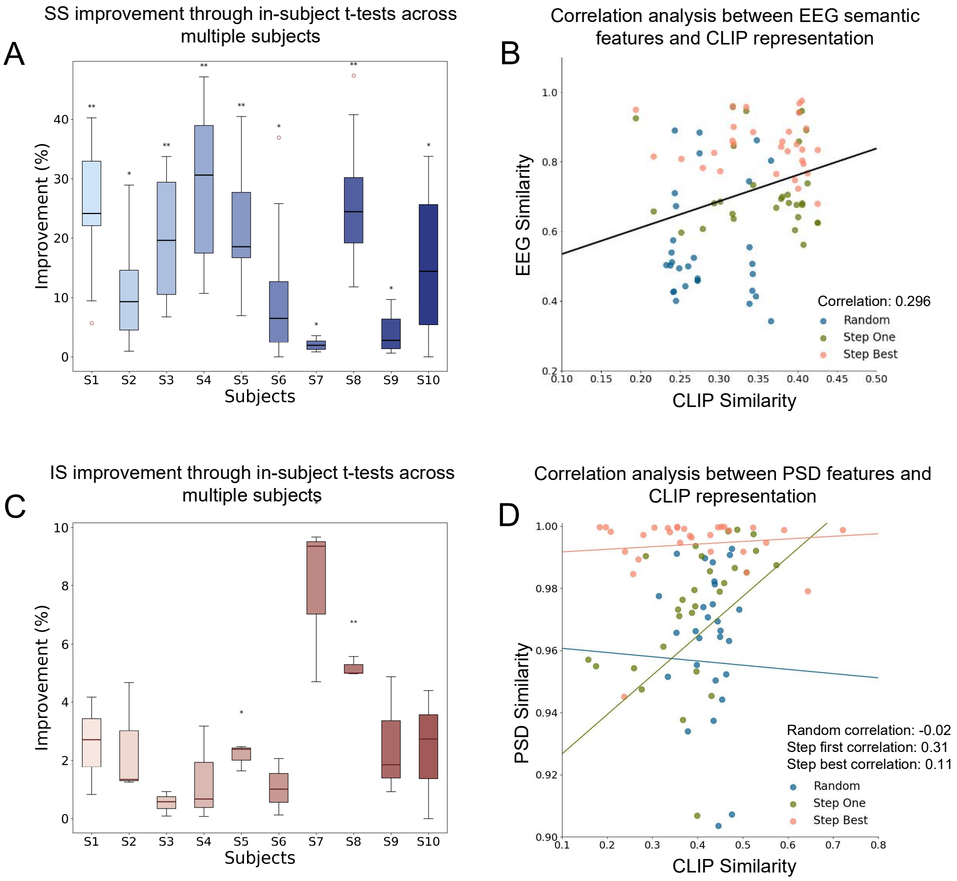

Figure A.3: **Improvement in similarity scores assessed via paired t-tests and correlation of similarity scores with targets across all subjects.** (A) Average EEG semantic representation scores (SS) for various target EEG semantic features. (B) The correlation of the similarity score with target between EEG semantic features across all subjects. (C) Average EEG response intensity scores (IS) for different target EEG PSD features. (D) The correlation of the similarity score with target between EEG PSD features across all subjects.

A.3 VALIDITY VERIFICATION OF SYNTHETIC EEG

To evaluate the performance of our EEG encoding models, we compare the synthetic EEG signals generated by two deep neural networks (DNNs)—AlexNet and CORnet-S—with real EEG data. Here's a step-by-step breakdown of how we processed and compared the data.

We selected 17 specific channels from the original 63-channel EEG dataset, focusing on those most relevant to visual processing. It ensured that we focused on neural regions most directly involved in responding to the visual stimuli. For each stimulus, we averaged the EEG signals across all trials, resulting in a representative dataset for each stimulus. This reduced the dimensionality of the data, making it easier to compare with synthetic data. We used a pretrained end-to-end encoding model to generate synthetic EEG signals based on the visual stimuli. The model captures the mapping between the visual input and the resulting EEG signals using deep neural networks. These synthetic signals represent the neural responses predicted by the model in response to the stimuli.

Table A.2: MSE Values for synthesized EEG

Subject	**Pretrained**		**Random Init**		**Average**
	AlexNet	**CORnet-S**	**AlexNet**	**CORnet-S**	
Sub-01	0.1095	0.1126	0.1161	0.0994	0.1094
Sub-02	0.0764	0.0788	0.0840	0.0994	0.0847
Sub-03	0.0787	0.0806	0.0816	0.0910	0.0830
Sub-04	0.0652	0.0664	0.0662	0.1011	0.0747
Sub-05	0.0493	0.0515	0.0704	0.0975	0.0672
Sub-06	0.0690	0.0719	0.0498	0.0966	0.0718
Sub-07	0.1267	0.1300	0.0914	0.1312	0.1198
Sub-08	0.0718	0.0727	0.1038	0.1165	0.0912
Sub-09	0.0529	0.0563	0.0781	0.0756	0.0657
Sub-10	0.1122	0.1151	0.0961	0.1149	0.1096
Average	0.0810	0.0832	0.0838	0.1023	0.0876

Table A.2 presents the mean squared error (MSE) between the synthetic EEG signals generated by AlexNet and CORnet-S, and the real EEG signals for 10 subjects. The MSE was computed for each individual test sample and then averaged across the entire test set. Lower MSE values indicate better alignment between the synthetic and real EEG signals.

From the comparison shown in the Figure A.4, the retrieval accuracy for S-S (both training and testing sets consist of generated signals) is significantly higher than other categories, including T-T (both training and testing sets consist of real signals), T-S (training set consists of real signals, testing set consists of generated signals), and S-T (training set consists of generated signals, testing set consists of real signals), under both AlexNet and CORnet-S models. This indicates:

Advantages of generated signals Supported by black-box ANN models (e.g., AlexNet and CORnet-S), generated signals perform significantly better in retrieval tasks compared to real signals. In particular, the highest retrieval accuracy for S-S demonstrates the consistency and model adaptability of generated signals in this retrieval task.

Model adaptability: Different ANN models (e.g., AlexNet and CORnet-S) show consistent superiority in the retrieval tasks for generated signals, indicating that generated signals are more easily captured and distinguished by black-box models.

In Figure A.5, we compute the variance across all samples and time points for each channel, providing a measure of the overall variability of the EEG signals in response to different visual stimuli and their temporal dynamics. This variance can help identify channels with the highest variability, which may be useful for selecting specific channels for further analysis or modulation.

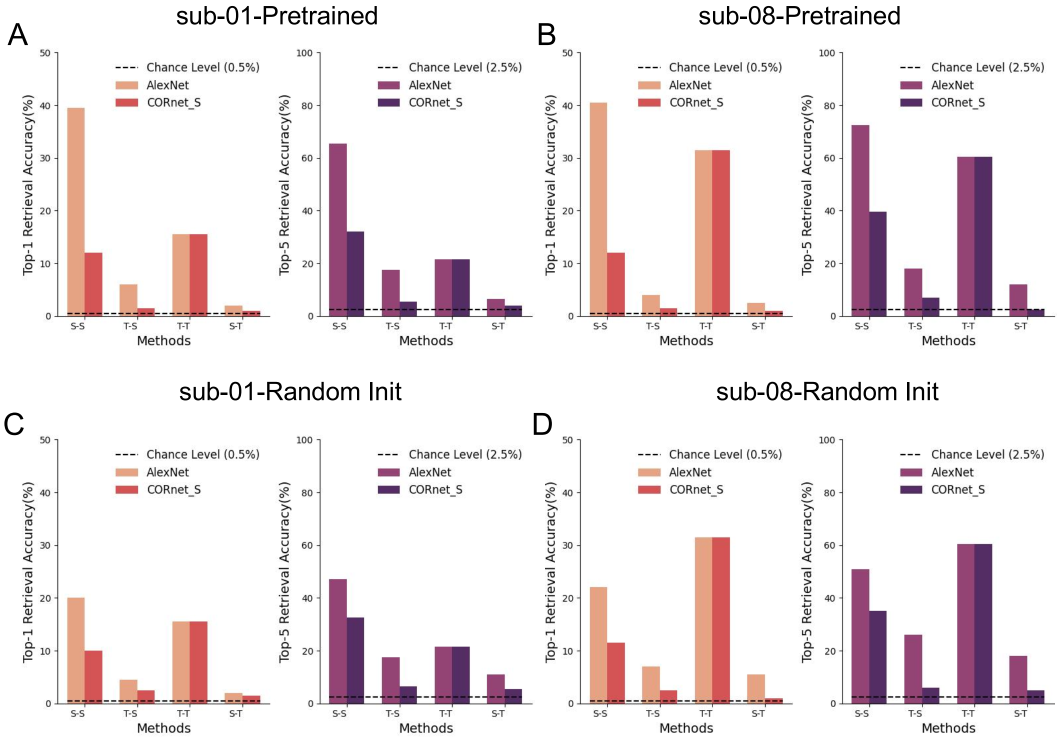

Figure A.4: Retrieval accuracy under different training and test datasets. Zero-shot retrieval performance of EEG data from different sources in Subject 1 and Subject 8 using ATM-S in different Settings. AlexNet and CORnet-S used in the first row were both pre-trained end-to-end models, and the second row was randomly initialized end-to-end.

In Figure A.6, we show the variance and standard deviation of the EEG signals computed across samples for each time point, and then averaged across channels. This analysis allows us to assess how signal variability evolves over time. By comparing the real EEG data with synthetic data generated by AlexNet and CORnet-S, we can evaluate how well each model captures the temporal variability present in the real EEG signals.

In Figure A.7, we compute the Pearson correlation coefficient between the averaged real EEG data and the synthetic data for each stimulus, measuring how well the synthetic data matches the real EEG on a per-sample basis. The histogram shows the distribution of correlation coefficients across all samples for both AlexNet and CORnet-S. A higher concentration of peaks near higher Pearson coefficients indicates better alignment between the synthetic data and the real EEG, reflecting superior model performance.

In Figure A.8, for each time point, we compute the Pearson correlation between the real EEG signal and the synthetic signals. This analysis enables us to visualize how well each model replicates the temporal structure of real neural responses to visual stimuli. Shaded regions in the plot represent the standard deviation across samples, showing the variability in model performance over time. The results provide a detailed view of how each model performs at different time points, highlighting which model more accurately captures the temporal dynamics of EEG signals.stimuli.

From the above analysis, we observe that both AlexNet and CORnet-S perform well, showing comparable results in terms of MSE, spatial (channel-wise) variability, and temporal (time-resolved) variability. The Pearson correlation analysis further confirms that they are able to synthesize EEG signals that align well with real data, with subtle differences in performance across models. These findings highlight the robustness of our EEG encoding models, demonstrating their ability that not only mimic the structural features of real EEG data but also capture the realistic variability seen in neural responses to visual stimuli. This suggests that our models are effective in approximating the neural representations underlying visual processing.

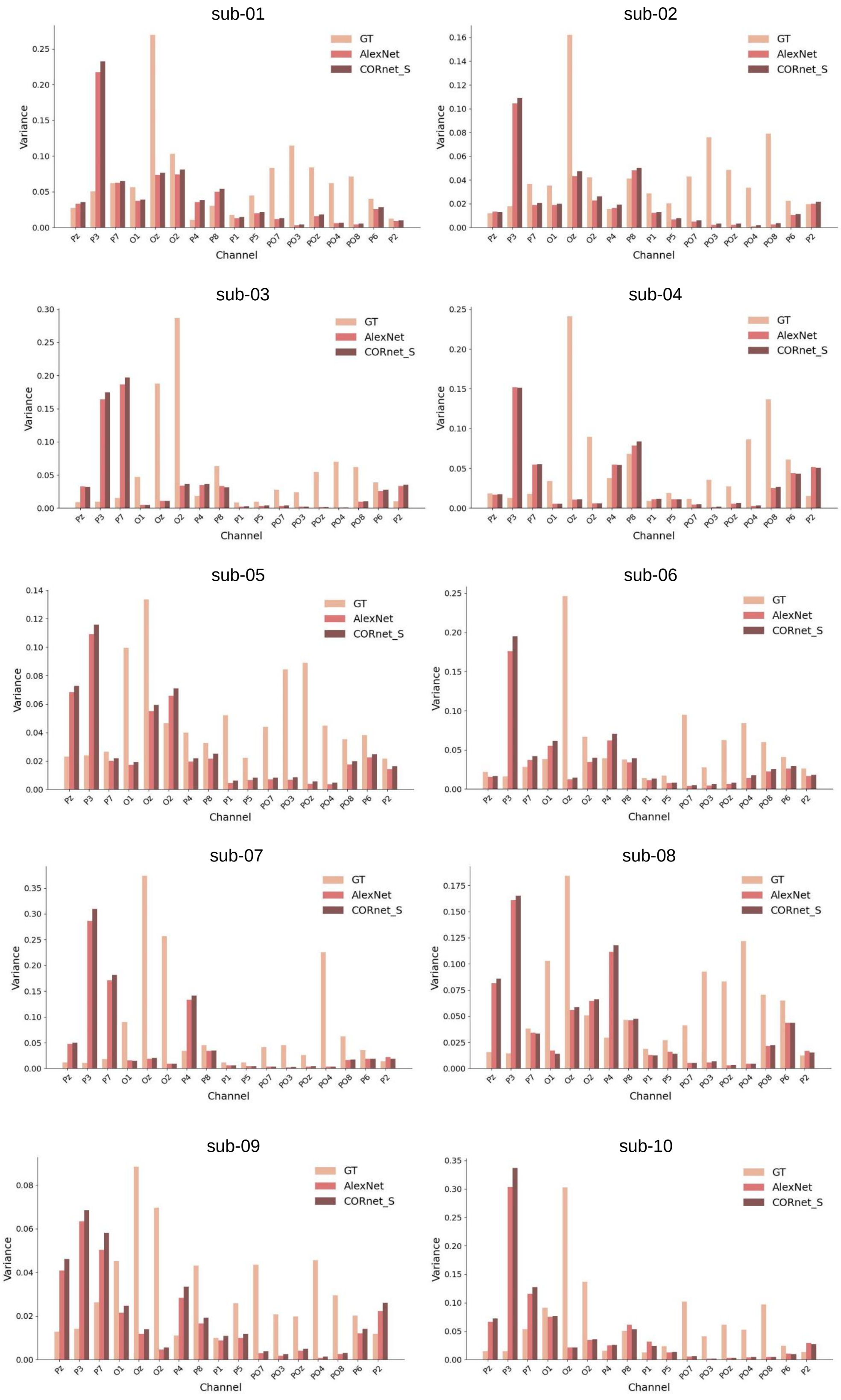

Figure A.5: Variance across different channels for different visual stimulus and temporal dynamics

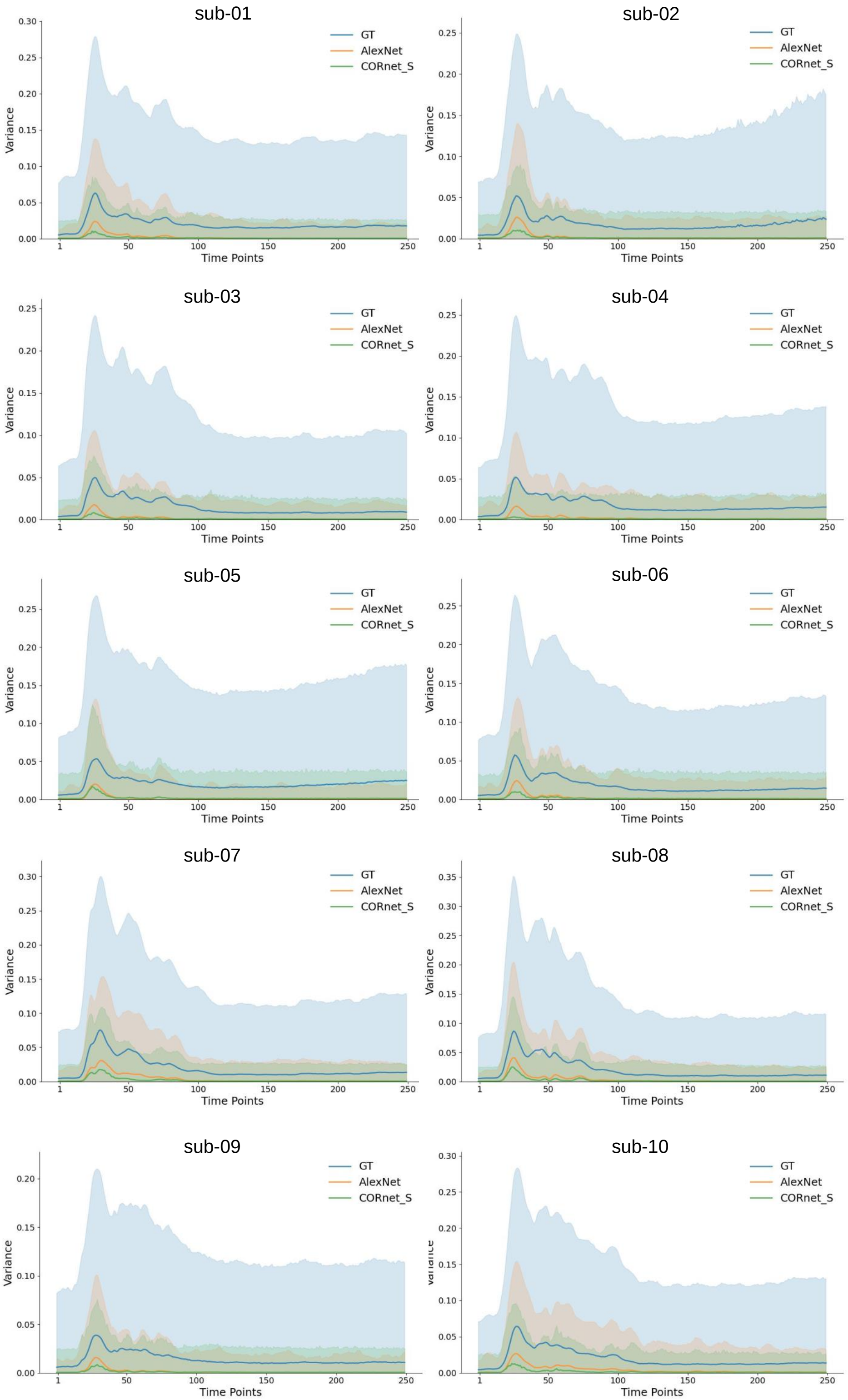

Figure A.6: Variance across different time points for different visual stimuli and channels.

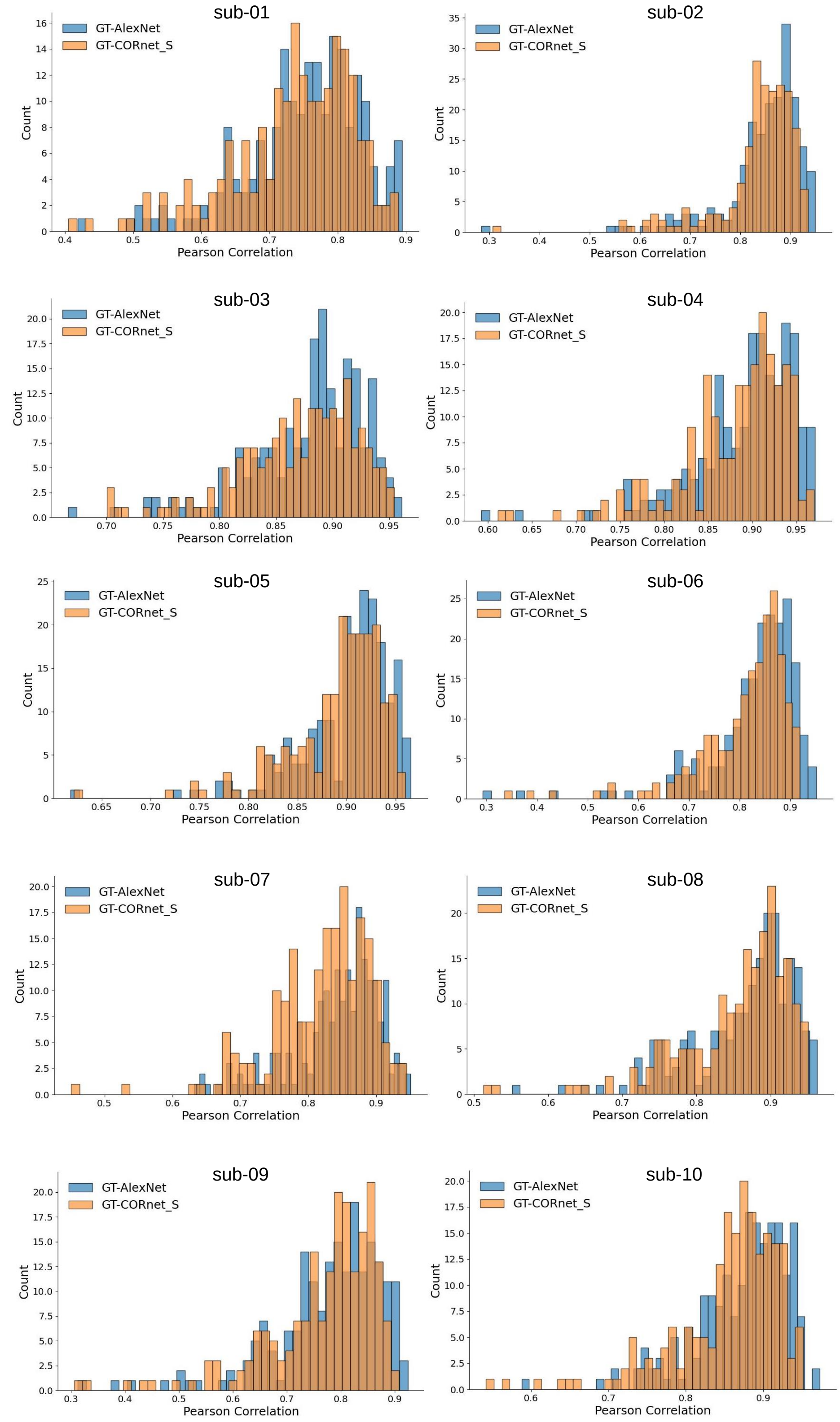

Figure A.7: Distribution of Pearson correlation coefficients across all sample pairs.

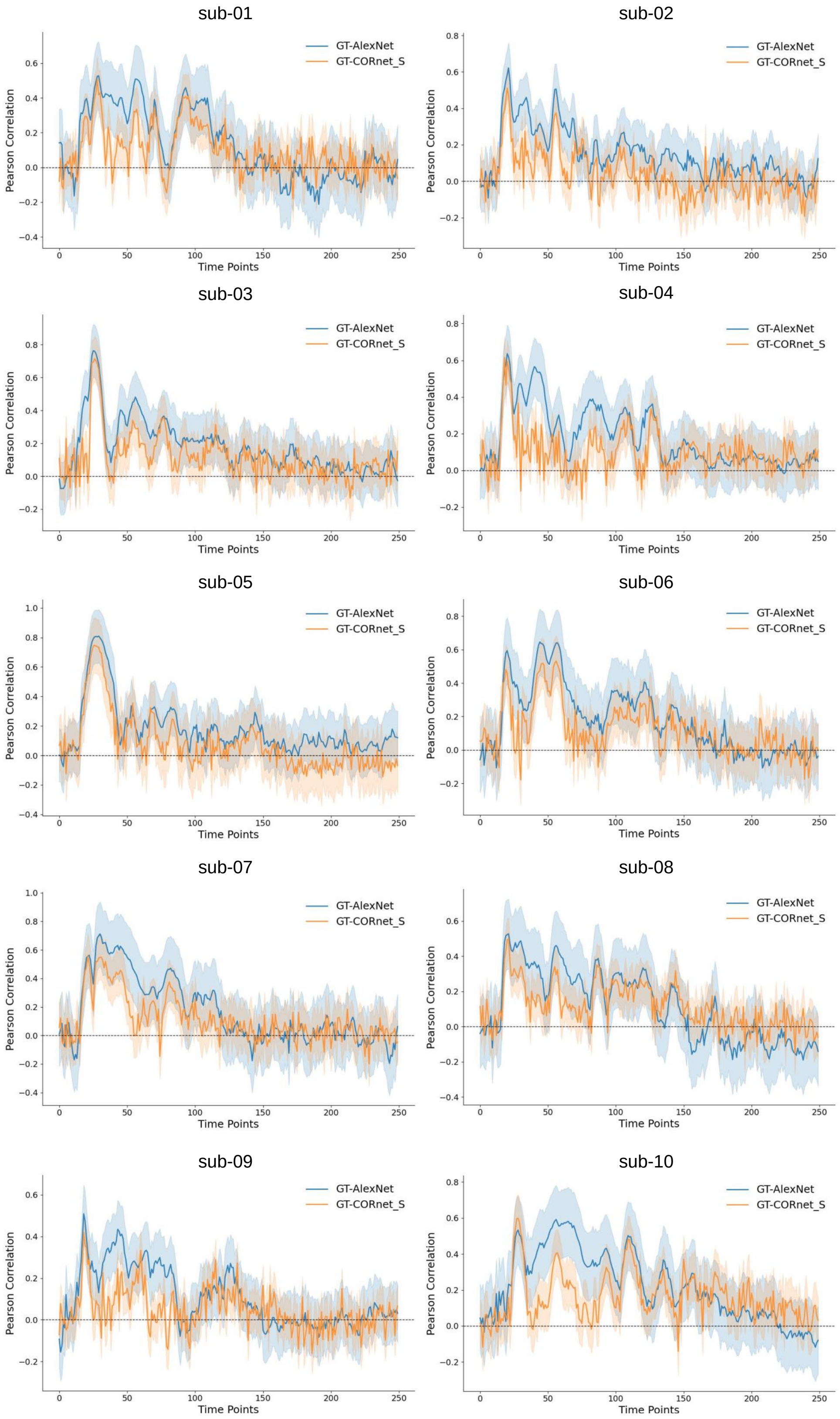

Figure A.8: Time-resolved Pearson correlation between ground truth EEG signals and synthetic EEG signals predicted by two neural network models (AlexNet and CORnet-S).

A.4 ADDITIONAL RETRIEVAL EXAMPLES OF SEMANTIC REPRESENTATION

A.4.1 MORE EXAMPLES OF RETRIEVAL

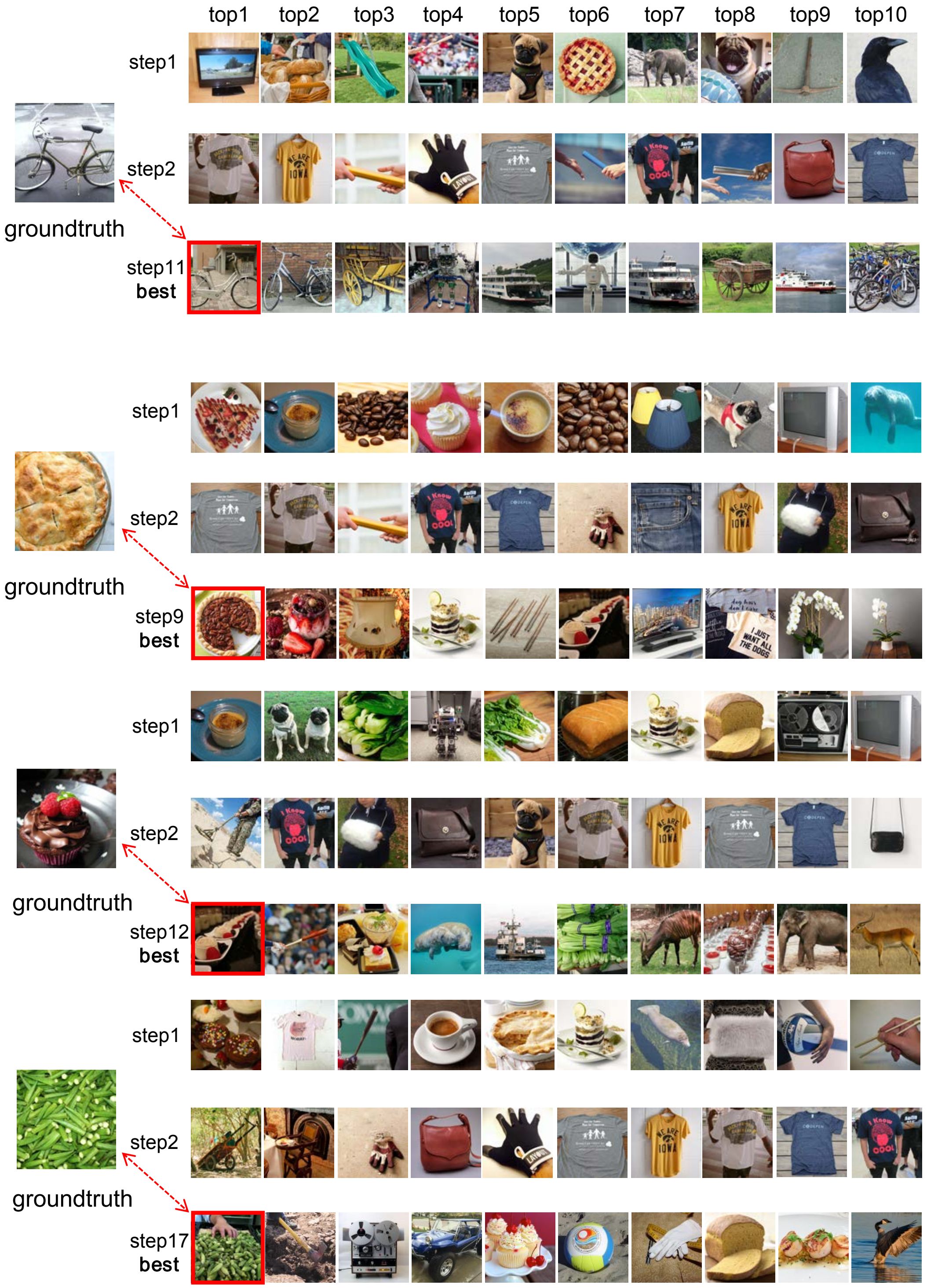

Figure A.9: **Some retrieval examples of Subject 8, 4, 4, and 1.** By setting different targets, we present examples where the stimulus retrieved at the end of the iterative optimization process increasingly approximates the true category.

A.4.2 SOME FAILURE EXAMPLES OF RETRIEVAL

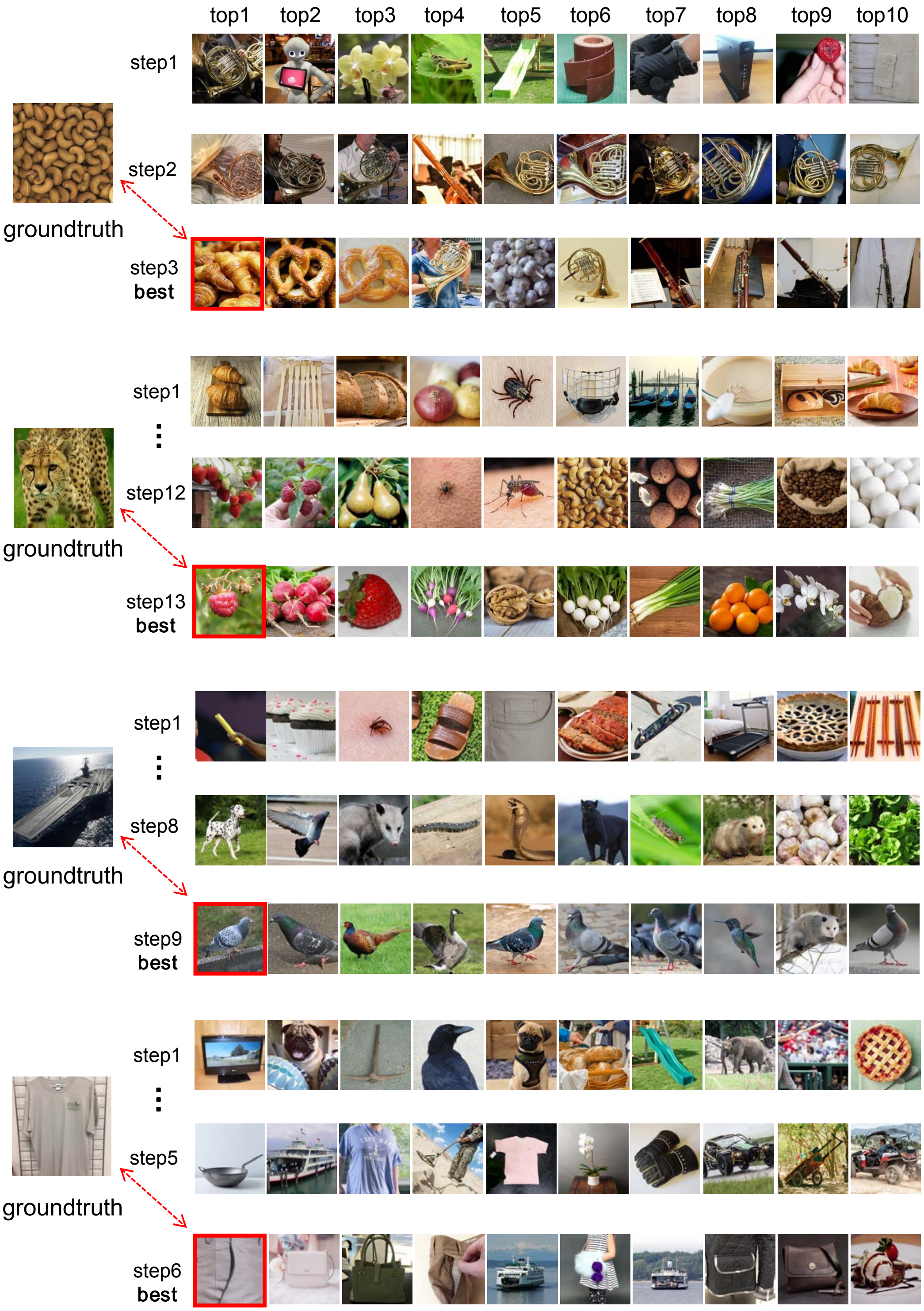

Figure A.10: **Some retrieval failure examples of Subject 8.** By setting different targets, we show examples where the stimulus retrieved at the end of the iteration is far from the true category. In these examples, the final retrieved stimulus exhibits varying degrees of similarity to the target image.

A.5 ADDITIONAL CONTROLLABLE GENERATION EXAMPLES OF PSD FEATURE

A.5.1 MORE EXAMPLES OF GENERATION

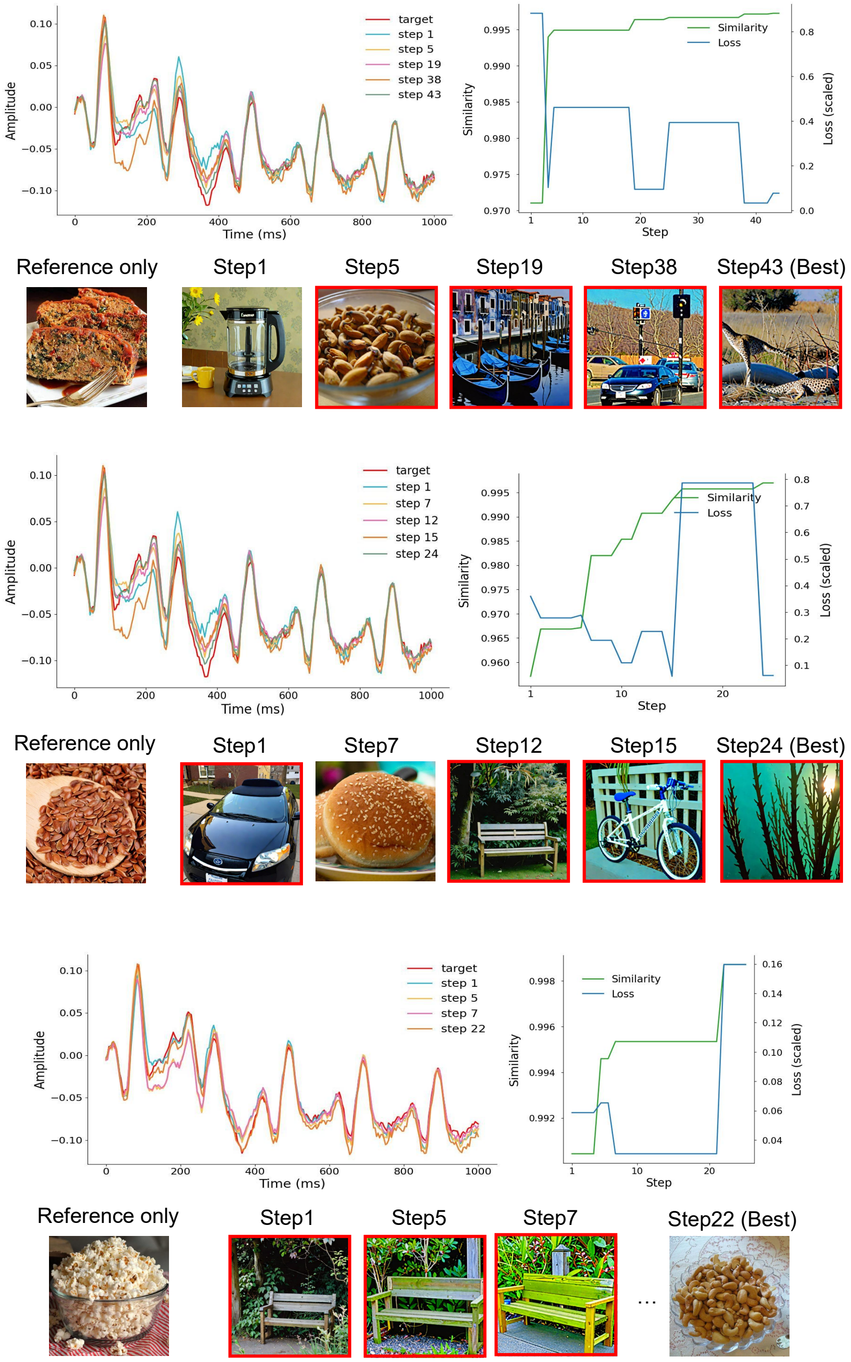

Figure A.11: **Illustration of the closed-loop iterative process for Subject 1.** Three distinct visual targets were presented, each based on a specific similarity measure (details in Target Features of EEG, Section 4.1), with new visual stimuli iteratively generated for each target. The left panel illustrates the time-domain evolution of neural responses across iterations. The right panel depicts the changes in similarity (green curve) and loss (blue curve, scaled) between the current stage features and the target features.

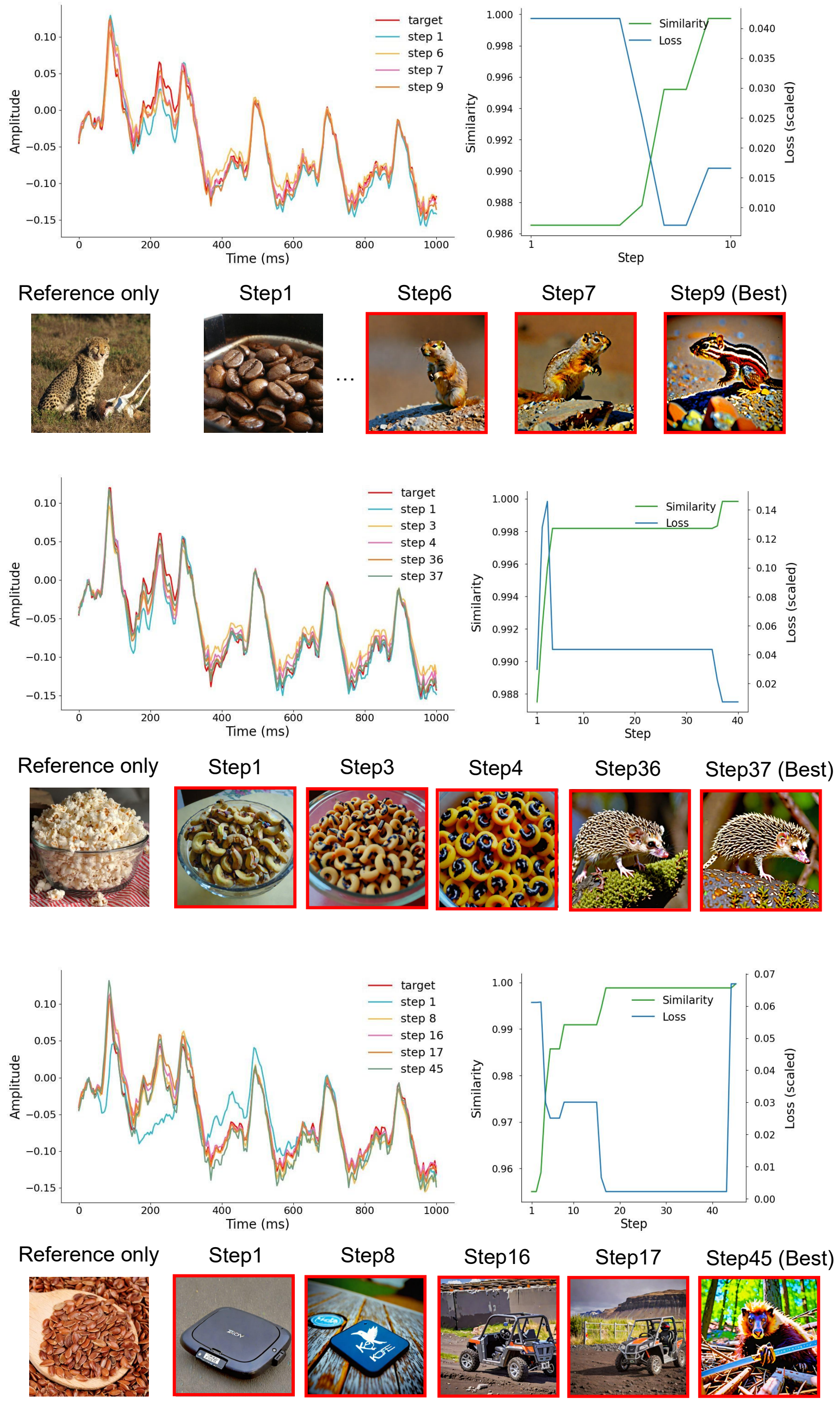

Figure A.12: **Illustration of the closed-loop iterative process for Subject 2.** Three distinct visual targets were presented, each based on a specific similarity measure (details in Target Features of EEG, Section 4.1), with new visual stimuli iteratively generated for each target. The left panel illustrates the time-domain evolution of neural responses across iterations. The right panel depicts the changes in similarity (green curve) and loss (blue curve, scaled) between the current stage features and the target features.

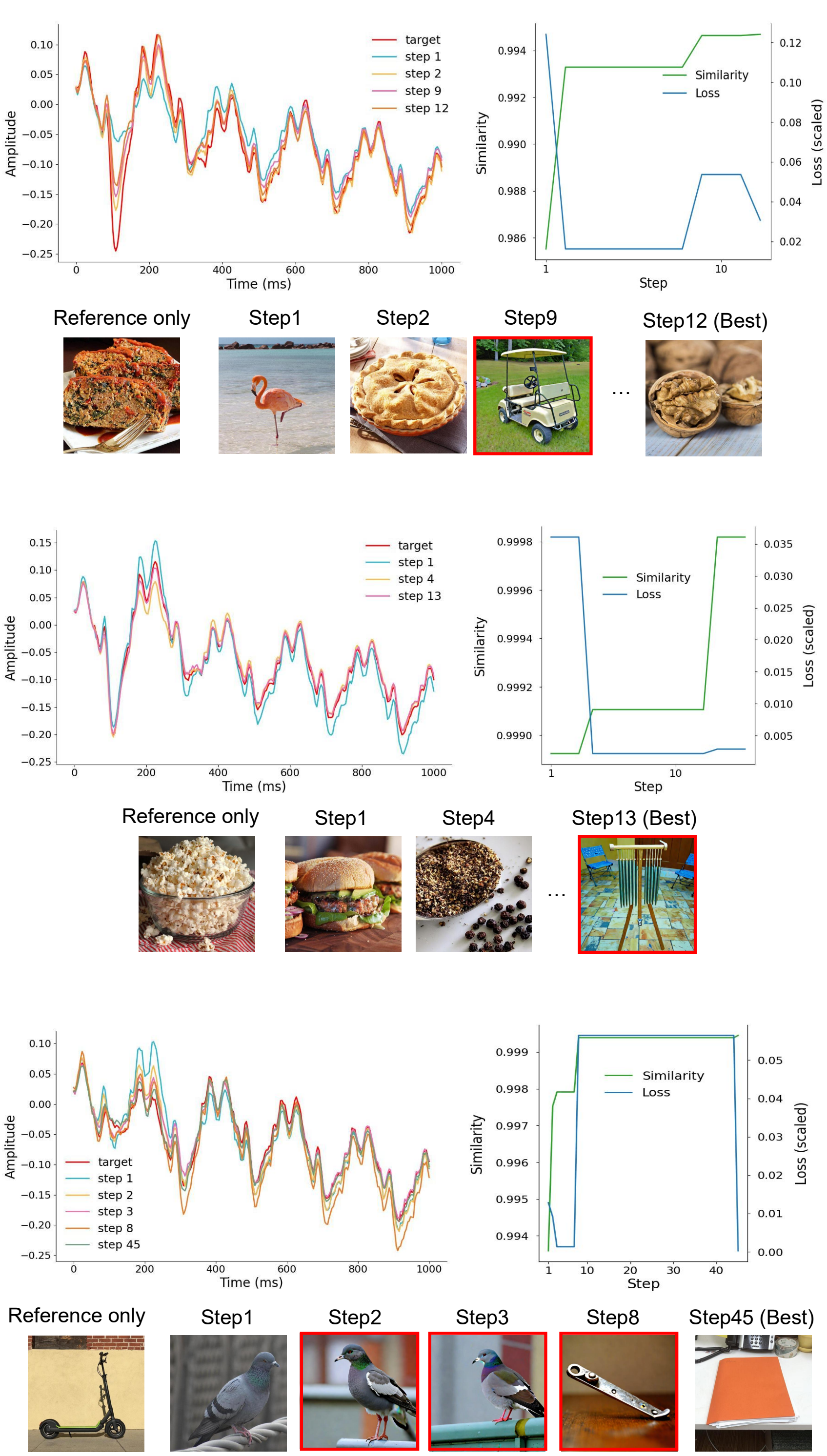

Figure A.13: **Illustration of the closed-loop iterative process for Subject 3.** Three distinct visual targets were presented, each based on a specific similarity measure (details in Target Features of EEG, Section 4.1), with new visual stimuli iteratively generated for each target. The left panel illustrates the time-domain evolution of neural responses across iterations. The right panel depicts the changes in similarity (green curve) and loss (blue curve, scaled) between the current stage features and the target features.

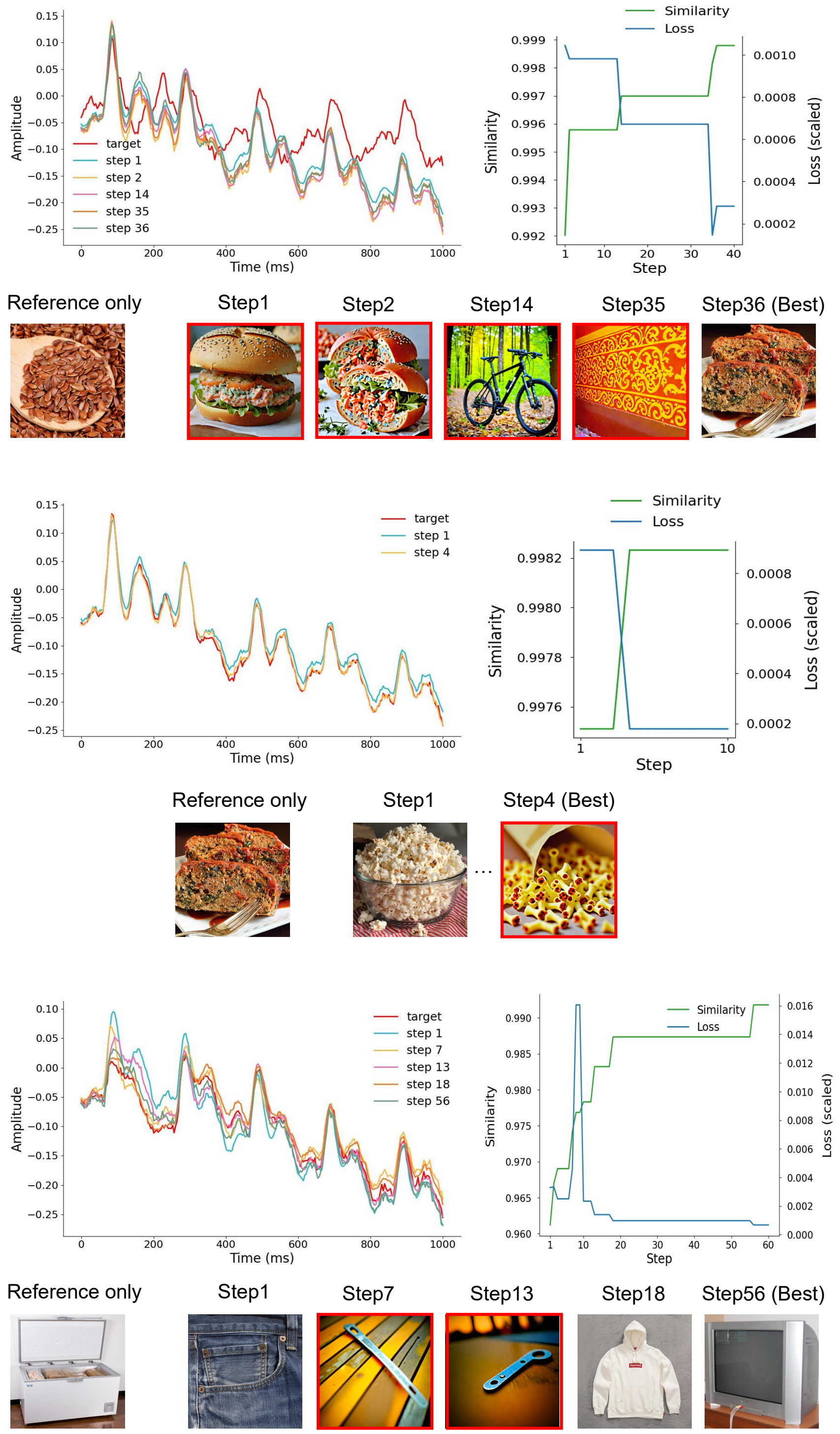

Figure A.14: **Illustration of the closed-loop iterative process for Subject 4.** Three distinct visual targets were presented, each based on a specific similarity measure (details in Target Features of EEG, Section 4.1), with new visual stimuli iteratively generated for each target. The left panel illustrates the time-domain evolution of neural responses across iterations. The right panel depicts the changes in similarity (green curve) and loss (blue curve, scaled) between the current stage features and the target features.

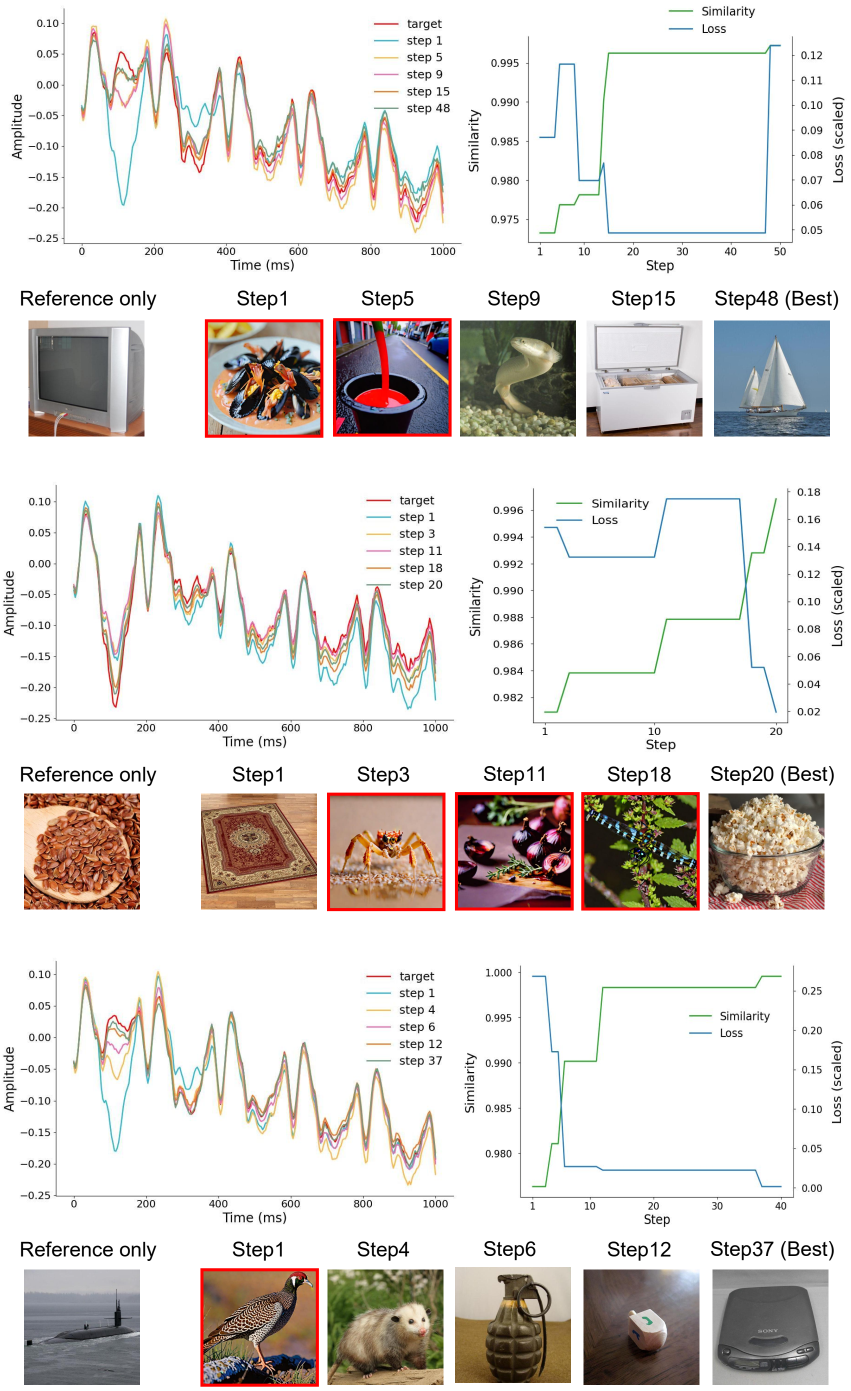

Figure A.15: **Illustration of the closed-loop iterative process for Subject 5.** Three distinct visual targets were presented, each based on a specific similarity measure (details in Target Features of EEG, Section 4.1), with new visual stimuli iteratively generated for each target. The left panel illustrates the time-domain evolution of neural responses across iterations. The right panel depicts the changes in similarity (green curve) and loss (blue curve, scaled) between the current stage features and the target features.

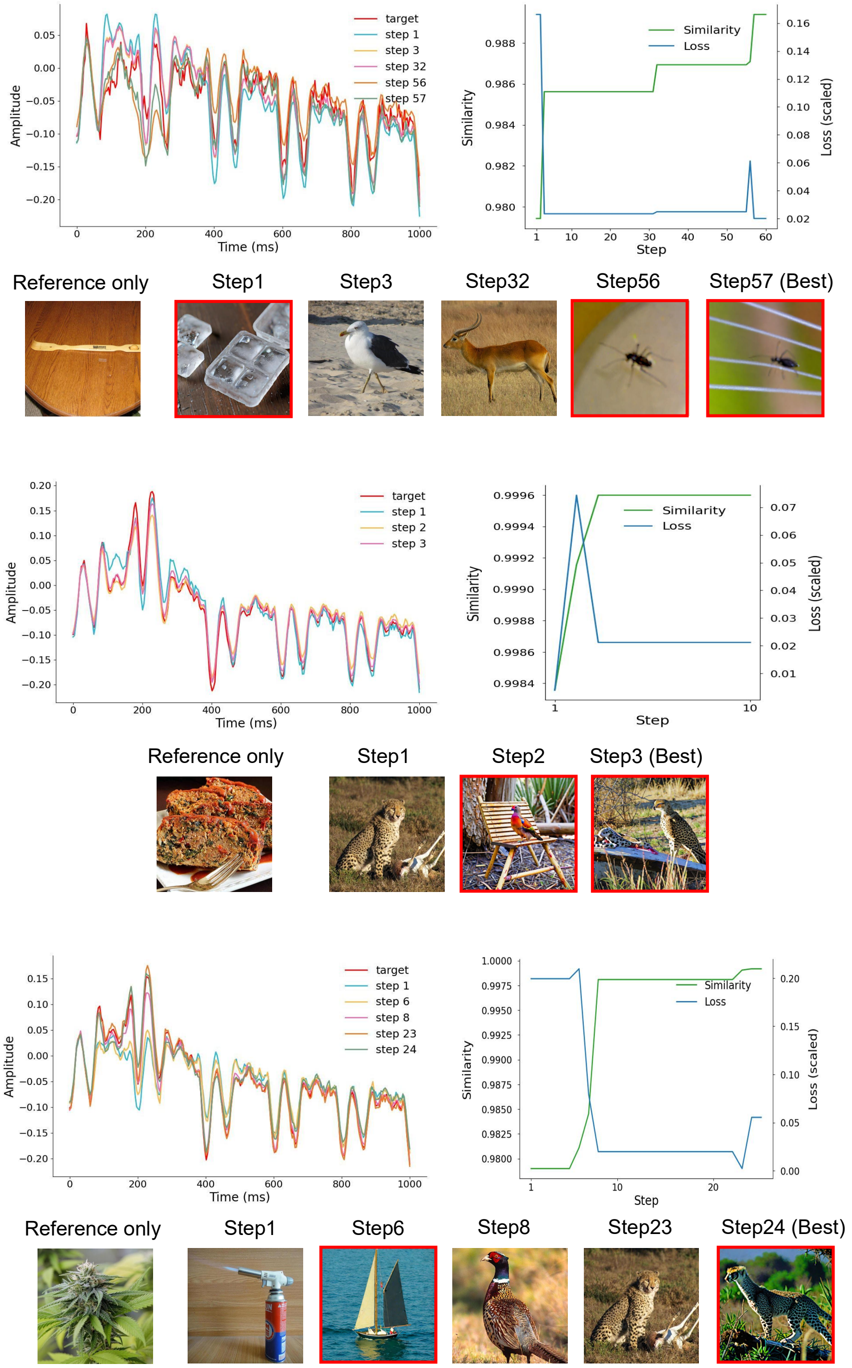

Figure A.16: **Illustration of the closed-loop iterative process for Subject 6.** Three distinct visual targets were presented, each based on a specific similarity measure (details in Target Features of EEG, Section 4.1), with new visual stimuli iteratively generated for each target. The left panel illustrates the time-domain evolution of neural responses across iterations. The right panel depicts the changes in similarity (green curve) and loss (blue curve, scaled) between the current stage features and the target features.

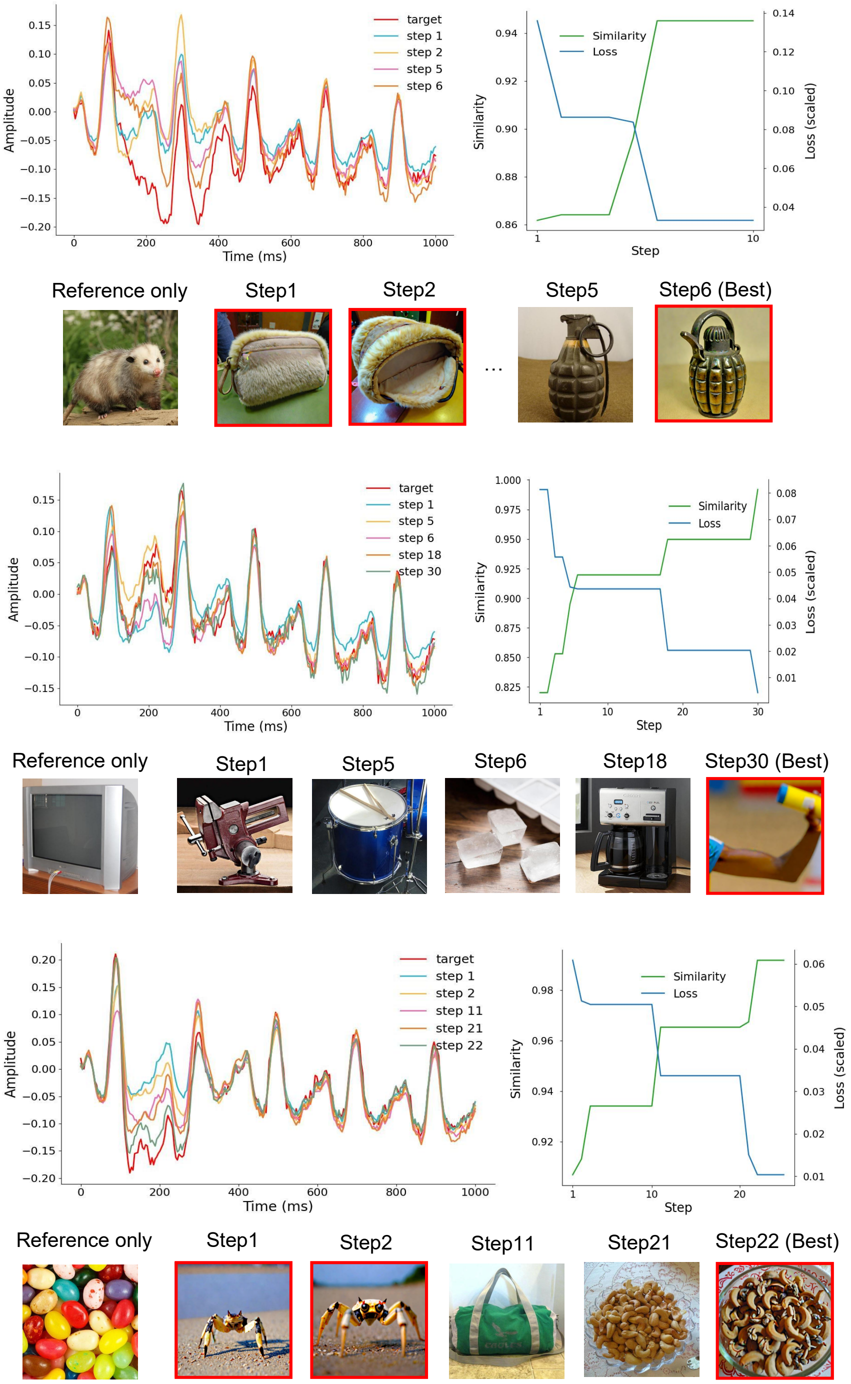

Figure A.17: **Illustration of the closed-loop iterative process for Subject 7.** Three distinct visual targets were presented, each based on a specific similarity measure (details in Target Features of EEG, Section 4.1), with new visual stimuli iteratively generated for each target. The left panel illustrates the time-domain evolution of neural responses across iterations. The right panel depicts the changes in similarity (green curve) and loss (blue curve, scaled) between the current stage features and the target features.

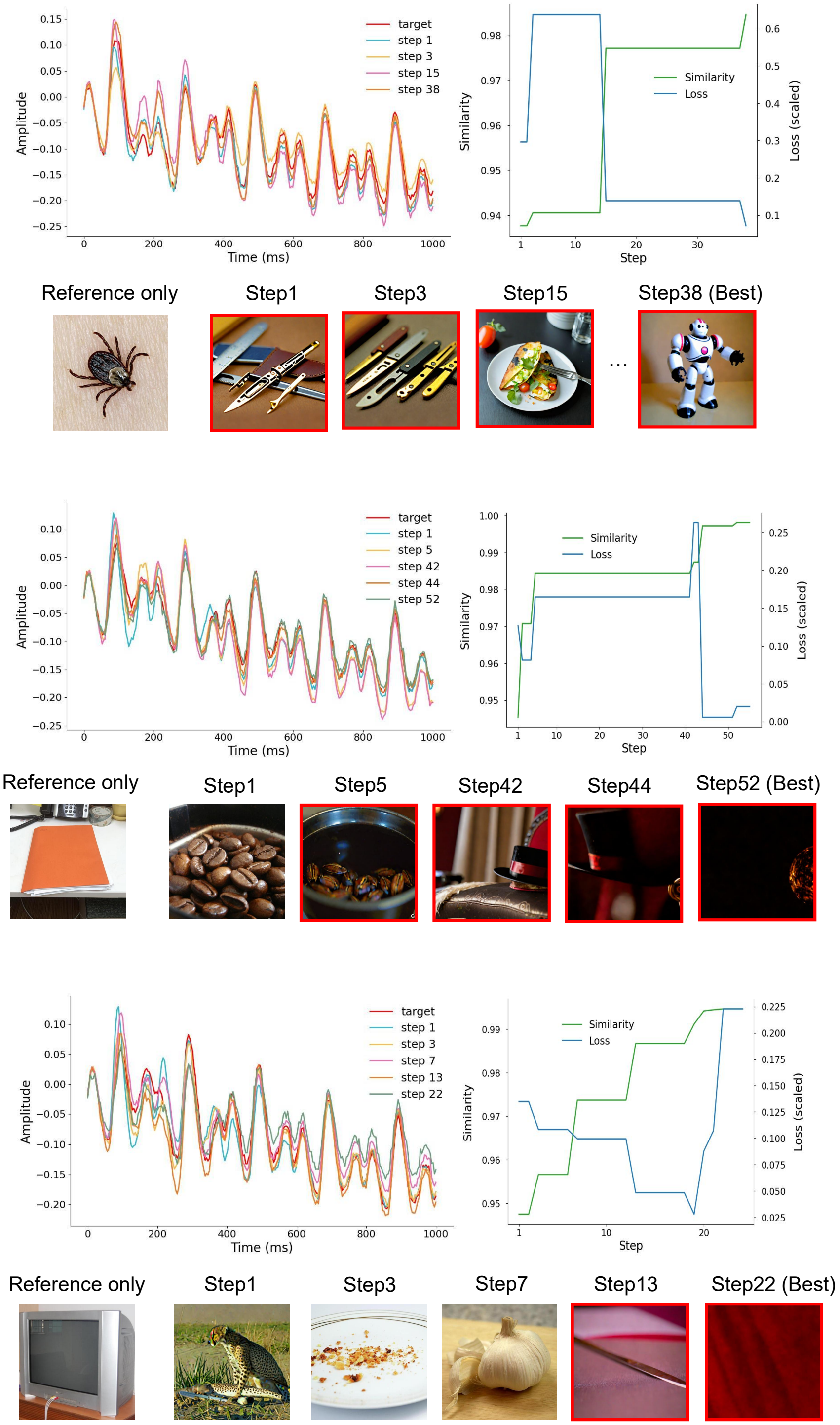

Figure A.18: **Illustration of the closed-loop iterative process for Subject 8.** Three distinct visual targets were presented, each based on a specific similarity measure (details in Target Features of EEG, Section 4.1), with new visual stimuli iteratively generated for each target. The left panel illustrates the time-domain evolution of neural responses across iterations. The right panel depicts the changes in similarity (green curve) and loss (blue curve, scaled) between the current stage features and the target features.

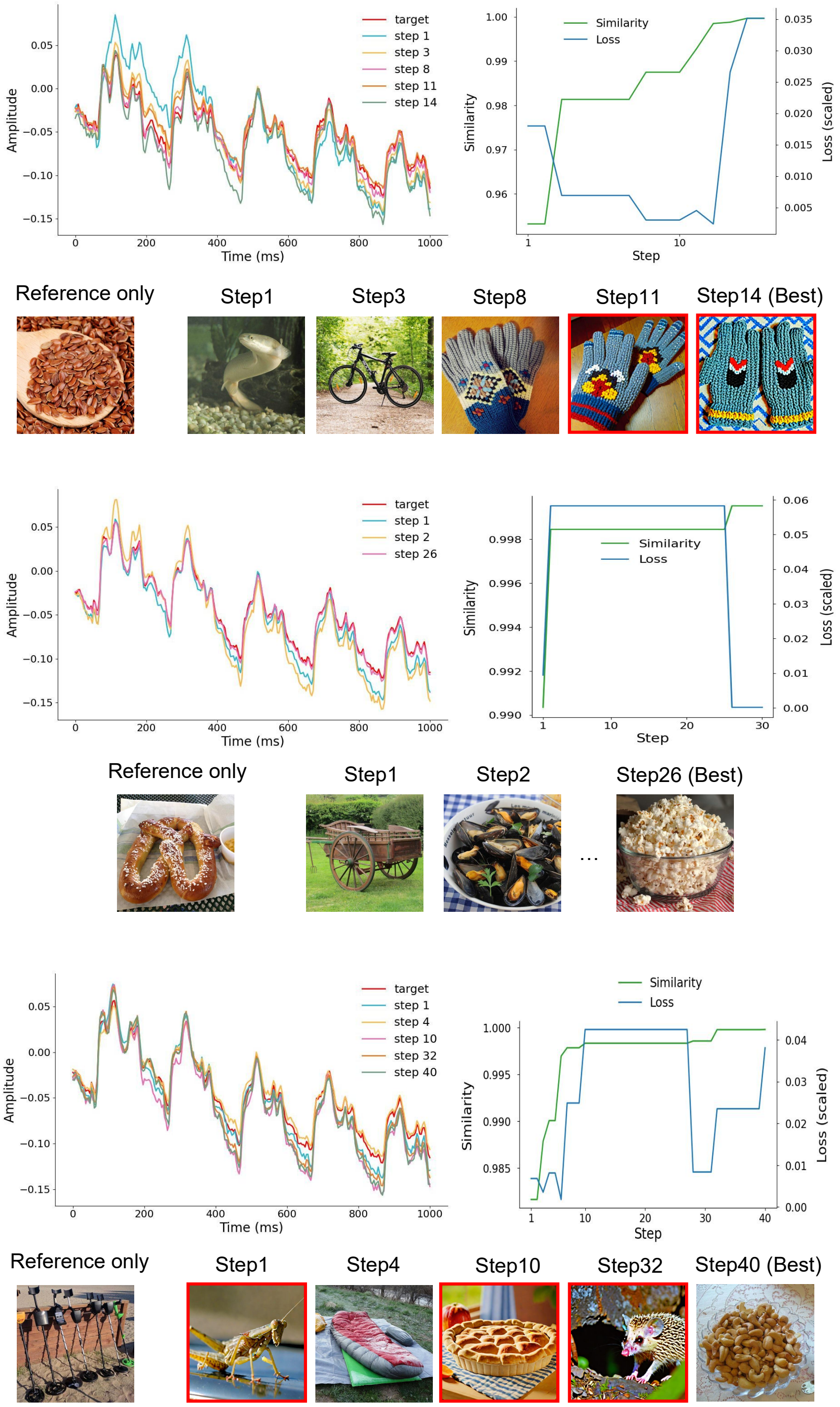

Figure A.19: **Illustration of the closed-loop iterative process for Subject 9.** Three distinct visual targets were presented, each based on a specific similarity measure (details in Target Features of EEG, Section 4.1), with new visual stimuli iteratively generated for each target. The left panel illustrates the time-domain evolution of neural responses across iterations. The right panel depicts the changes in similarity (green curve) and loss (blue curve, scaled) between the current stage features and the target features.

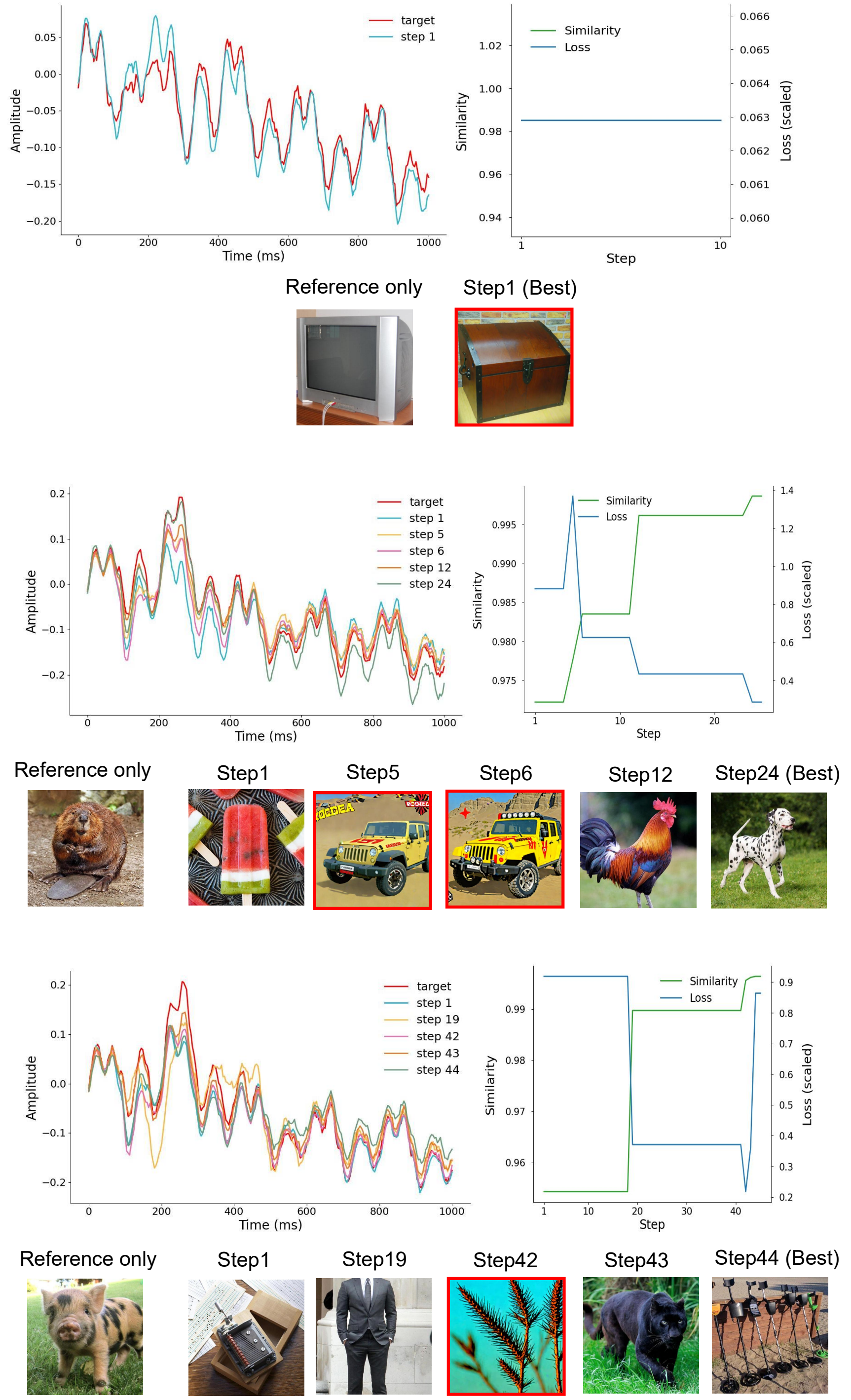

Figure A.20: **Illustration of the closed-loop iterative process for Subject 10.** Three distinct visual targets were presented, each based on a specific similarity measure (details in Target Features of EEG, Section 4.1), with new visual stimuli iteratively generated for each target. The left panel illustrates the time-domain evolution of neural responses across iterations. The right panel depicts the changes in similarity (green curve) and loss (blue curve, scaled) between the current stage features and the target features.